ION DELIVERY USING ALKALI HALIDE NANOPARTICLES FOR TUMOR THERAPY AND OSTEOARTHRITIS TREATMENT

by

TREVER JONATHAN TODD

(Under the Direction of Jin Xie)

ABSTRACT

Sodium chloride and lithium fluoride nanoparticles were synthesized and evaluated for their ability to kill cancer cells and protect chondrocytes from damage in osteoarthritis models, respectively. Sodium chloride nanoparticles were fabricated by two methods and yielded crystalline cubes that are colloidally stable in non-polar organic solvents. TEM, SEM, XRD, ICP-OES, EDS, and DLS were used to characterize the particles. The particles were endowed with aqueous stability using a phospholipid coating and subsequently introduced to tumor cells or injected into animals. Toxicity was observed in vitro with a LC_{50} of ~64 µg/mL Na^+ added from the particles. Controls of PBS, aqueous NaCl, and free phospholipid showed no increased toxicity. Notably the toxicity is dependent on the duration the particles have been in solution. Particles that are immediately added into cells after dispersion in aqueous solution are significantly more toxic than particles that have been allowed to rest in solution. After 8 hours the particles are only minimally toxic and all observable affects are absent after 24 hours. The toxicity observed with the particles was found to proceed through a necrotic pathway, with only minimal contributions from apoptosis.

Lithium fluoride nanoparticles were synthesized by a precipitation reaction in a mixed solvent system of ethylene glycol and poly(ethylene glycol). The particles were coated with a silica shell to protect from rapid aqueous degradation and attack by extracellular calcium. ICP-MS found that the coated particles slowly release lithium over the course of 48 hours. When added to chondrocytes in vitro, the particles down-regulated the expression of damaging cytokines MMP-1, -3, and -13. In vivo, the particles inhibited damage to the joint area in rat osteoarthritis models comparable to injection of 10x the concentration of aqueous LiCl. It was concluded that the slow release of lithium from the relatively large nanoparticles was responsible for the increased efficiency of therapeutic effect.

INDEX WORDS: alkali halide, sodium chloride, lithium fluoride, nanoparticles, tumor therapy, osteoarthritis, ion delivery

ION DELIVERY USING ALKALI HALIDE NANOPARTICLES FOR TUMOR THERAPY AND OSTEOARTHRITIS TREATMENT

by

TREVER JONATHAN TODD

BS, Armstrong State University, 2010

A Dissertation Submitted to the Graduate Faculty of The University of Georgia in Partial Fulfillment of the Requirements for the Degree

DOCTOR OF PHILOSOPHY

ATHENS, GEORGIA

2016

ION DELIVERY USING ALKALI HALIDE NANOPARTICLES FOR TUMOR THERAPY AND OSTEOARTHRITIS TREATMENT

by

TREVER JONATHAN TODD

Major Professor: Jin Xie

Committee: Vladimir Popik
Sergiy Minko

Electronic Version Approved:

Suzanne Barbour
Dean of the Graduate School
The University of Georgia
August 2016

DEDICATION

I cannot begin to list the people who I am thankful for assisting, carrying, and sometimes dragging me down the path that has culminated in this document and it is to these persons whom dedicate this dissertation. Specifically, I credit (and occasionally curse) Joseph Traywick and Joshua Smith for guiding me into the study of chemistry. Jin Xie has been an excellent mentor and leader, and I cannot overestimate the appreciation I have for his guidance. My parents, Bill and Cherie, and my sister, Michelle, have always encouraged me to follow my passions and I would not have been able to without their support. I owe Mackenzie more than I could possibly hope to transcribe through any medium, but our travels, journeys, and adventures over the years in Athens have been the most important experiences of my life.

ACKNOWLEDGEMENTS

I thank the University System of Georgia for providing me with the opportunity to study science over the past nine years. Also, funding from UGA and NIH has been most appreciated. Many thanks are extended to the Advanced Materials Research Lab at Clemson for the ability to use their facilities. I greatly appreciate all the work done by John Yu's lab on the NaCl project and Li Zheng's efforts on analysis of LiF.

TABLE OF CONTENTS

Page

LIST OF FIGURES

Page

LIST OF TABLES

Page

CHAPTER 1

INTRODUCTION AND LITERATURE REVIEW

Introduction

Homeostasis of ions across cellular membranes is one of the most critical parameters to ensuring healthy cellular function and is preserved across all kingdoms of life. In comparison to the extracellular space, the intracellular cytoplasm is characterized by an overabundance of potassium and lower concentrations of sodium, chlorine, and calcium[1]. The differences in ion concentration provide energy for amino acid and sugar transport across the cell membrane, maintenance of cellular pH, control of cell volume, and allows the conduction of electrical impulses in excitable cells[2-5]. This asymmetric balance of ions is generated and maintained by numerous energy-independent channels that allow ions to pass down their concentration gradient and energy-dependent pumps the transport ions against the gradient. Among the ion pumps, the Na^+/K^+ ATPase pump is one of the most critical[6]. In average cells it is estimated to consume ~20% of a cell's total ATP consumption. In active neurons this increases to ~60%[7].

Given the importance of ion homeostasis, its disruption leads to alteration cell function and viability. Minor dysregulation of ion homeostasis from malfunctioning ion transport has been associated with diseases ranging from heart arrhythmia to cystic fibrosis to neurological disorders [8,9]. At more extreme levels of ion concentration disruption, cellular death rapidly follows[10]. The potential benefits of translating this

mechanism into therapeutics are plentiful. Ionophores, which are small molecules that transport ions with their concentration gradient across cell membranes are the most successful application ion homeostasis disruption. Originally used as antibiotics for poultry and ruminants, recent research has demonstrated that ionophores have numerous anti-cancer abilities including directly killing cells, sensitizing resistant cell lines to chemotherapy and radiotherapy, and selectively killing cancer stem cells[11,12].

This following chapter will briefly cover an introduction to cellular ion homeostasis and how it is established. The remaining portion will detail the therapeutic uses and outcomes of ion delivery as it relates to sodium, potassium, chlorine, and lithium. Monovalent species excluding hydrogen are the focus of this work and chosen due to their applicability to subsequent chapters of this thesis. A brief introduction to nanoparticle based therapy will conclude this chapter.

Ion Homeostasis

The generation and upkeep of heterogeneous ion concentrations across the cellular membrane is of critical importance to cellular function and viability. Nearly every organism maintains high intracellular concentrations of potassium whereas sodium, chlorine, and calcium are kept at low amounts [1]. This contrasts to the extracellular environment, especially in animals, where concentrations of sodium, chlorine, and calcium are relatively high and the potassium levels are low. As an example, in human cells intracellular concentrations of potassium are approximately 20 fold higher than extracellular amounts[13]. However intracellular amounts of, sodium, chlorine, and calcium are 10, 25, and 10000 times lower, respectively, than the extracellular environment[1]. These ion gradients are responsible for numerous cellular functions

including providing energy for amino acid transport across the cell membrane[3,14,15], maintenance of cellular pH[4,16], control of cell volume[2,5], and allowing the conduction of electrical impulses in excitable cells[17,18]. Because the cell membrane is impermeable to charged ions, a multitude of ion-transporting transmembrane proteins are required for the asymmetric natural ion balance; including symporters, antiporters, uniporters, ion channels, and ion pumps[19]. The following section will cover two main categories of ion transporters; energy-independent channels and energy-dependent pumps.

The energy-independent channels are so named because they allow the transport of ions down their concentration gradient[17]. This entropically favored transfer would quickly equilibrate ion concentrations across the membrane if not for the cell's membrane potential and strictly controlled 'gates' that only open in response to stimuli such as voltage[9]. Because the transfer of ions through an open channel is dependent only on the difference in concentration between the extra-and intra-cellular spaces—the rate of transfer through a channel can be very high, up to 1 $x10^8$ ion/s [20]. Controlled opening and closing of ion channels regulates the ion flow and can quickly disrupt the cell membrane potential in a localized area.

Careful regulation of this process is the mechanism by which neurons of the central nervous system and myocytes of the muscles are fired [21]. In neurons, external stimulation of a slight increase in membrane potential (~10 mV) causes sodium channels to open, rapidly increasing the cell membrane potential of that area from -70 mV to + 20 mV. As the membrane potential increases to 20 mV the sodium channels close and potassium channels open, quickly bring the membrane potential back to the resting state, -70 mV. Notably, during this process the actual number of ions transferred

is relatively small as compared to the total amount available. The large swings in potential are due to the rapid changes in permeability of sodium and potassium. While the total transfer of ions is relatively low for each cell excitation, the sheer number of events that takes place would gradually erode the ion gradient and prevent further signaling. To generate and maintain the asymmetric concentrations another method is required.

Energy-dependent ion pumps are the main mechanism by which the balance of ions is created[22]. As with channels, the pumps facilitate the movement of ions across the cell membrane. Unlike channels, these pumps almost always transport ions against their concentration gradients. This transport is thermodynamically unfavored and requires the hydrolysis of one molecule of adenosine triphosphate (ATP) to adenosine diphosphate(ADP). That process, concerted binding, and protein structural changes frequently allow the transport of multiple ions, and many pumps also transport two or more ionic elements. A prototypical example of this type is sodium/potassium ATPase (Na^+/K^+-ATPase).

Originally discovered in the 1950s, Na^+/K^+-ATPase has since become one of the most widely studied and best understood ion transporters[6]. It is estimated that nearly 20% of a cell's energy expenditure is used to power this pump. In active neurons, this can rise to 50 or higher[7]. Na^+/K^+-ATPase's method of action first binds three sodium ions in the intracellular space and then coordinates a molecule of ATP[23]. ATP is hydrolyzed which leads to conformational changes in the enzyme and exposes the sodium ions to the extracellular environment where they are released. This process exposes potassium binding sites, which when filled, induces a structural change

inserting the potassium ions into the cell. A summary of this process is shown in **Figure 1.1**.

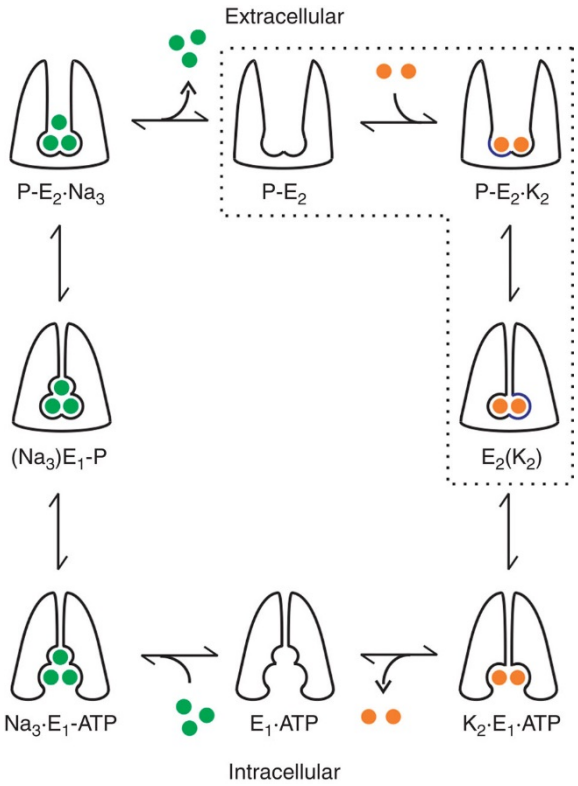

Figure 1.1 Schematic representation of Na^+/K^+-ATPase mechanism[23].

With the established importance of Na^+/K^+-ATPase it is of little surprise that its impairment or dysregulation is associated with a number of disease states [6,24,25]. In addition, ouabain, a glycoside that inhibits Na^+/K^+-ATPase, was used as the basis of poisons for hunting in eastern Africa[26]. Further studies have found that instead of altering the function of naturally expressed protein ion transporters there exist small molecules that can modulate ion delivery independent of these endogenous pumps and channels.

Ionophores

Molecules that fit this definition, ones that facilitate the transport of ions across cellular membranes independent of endogenous processes, are known as ionophores. Of the more than 120 known natural ionophores, more than half are moderate mass (~700-1000 Da.) polyether compounds[11]. When exposed to cations with both the correct charge and size, these flexible polyethers contort to enclose the ion[27]. This chelation is driven by the semi-encapsulation and binding of numerous oxygen containing functional groups. In many cases the ionophores have a single negative charge which neutralizes the positive charge of an alkali metal. The non-polar backbone of the polyether shields the complex and thus the cation from the charged surfaces of cellular membranes. This allows the rapid transport of ions across lipophilic barriers, which disrupts the carefully controlled ion balance.

Many of these molecules, their associated mechanisms, and crystal structures have been known and used commercially for some time[28]. These polyether ionophores have been and continue to be used as antibiotics in poultry and ruminant feed stock[12]. Given the slow digestion of the plant material consumed by these species, a significant portion of the available energy is consumed by microfauna resulting in reduced animal growth and lower profitability[29]. Ionophores are able to inhibit the production of methane and decrease protein degradation by many of the most causative microorganisms. With the translation of several antibiotics such as bleomycin, doxorubicin, and daunorubicin into anti-cancer drugs, a number of these antibiotic ionophores have been suggested as possible chemotherapeutics in humans[30]. Indeed, recent research has indicated that in

addition to their antibiotic properties, many of these polyether compounds display potent anti-tumor activity.

The next sections will describe the causes and effects of disruption of the natural homeostasis in cells with regards to specific ions. Sodium and potassium have a long history demonstrating their positive effects of unregulated ion toxicity to bacteria and tumor cells. Whereas, chloride has only been recently suggested as a therapeutic modality. Lithium has shown benefits to mental health for many years, but recent research indicates that it can be used in other illnesses as well.

Sodium

As briefly described above, sodium transporting ionophores were first used in poultry feedstock but quickly became a standard in ruminant food as well[31-33]. Of the sodium ionophores, monensin is the most commonly used and can improve the gain in cattle mass by 10% [12,29]. This effect is due to the inhibition of a number of gram-positive bacterial in the animals' digestive systems that produce by-products which consume nutrients and energy before the host animal can absorb them. The two most significant inhibited by-products are the generation of hydrogen which leads to methane synthesis, and the fermentation of amino-acids into ammonia[34-36]. The bacteria species that are most affected by this process lack a cell wall allowing the rapid integration of ionophores into the bacterial membranes and thus suffer from a higher rate of ion homeostasis disruption[34,37,38]. When tested in *S. bovis* cells, monensin resulted in an increase of intracellular sodium from 16 mM to 322 mM[10,39]. Correlated with this increase of cellular sodium, there was a decrease of ATP from 3.2mM to 1.8mM. This decrease likely stems from the excessive activation of the Na^+/K^+ ATPase pump

attempting to normalize the sodium concentration[29]. The decrease of cellular potassium from 613mM to 134mM supports this hypothesis. Ultimate cell death is attributed to starvation of ATP, the loss of the Na^+/K^+ ion gradient, and cellular swelling.

With the favorable antibiotic properties of monensin and the successful translation of several antibiotics to anti-tumor therapeutics, the drug was evaluated as a potential anti-cancer agent[30,40]. In one of the seminal studies investigating this possibility, monensin was introduced to a number of acute myelogenous leukemia cell lines[41]. The drug was found to inhibit nine of the ten tested cell lines by more than 50% at 0.5 µM. High fluorescence from annexin V-FITC and loss of signal from the mitochondrial transmembrane potential dye Rhodamine 123 suggests depolarization of the mitochondria which leads to apoptosis. However, monensin's high lipophilicity leads to a short half-life in vivo which necessitates loading into formulations for delivery to tumors[42]. These monensin loaded liposomes and nanoparticles have seen extensive use as potentiators for immunotoxins as well as increasing drug efficiency in resistant cell lines[43-45]. A more recent, high throughput study found that monensin was one of four chemicals of 4910 tested that could selectivity inhibit prostate cancer growth[46]. As with previous studies, the influx of sodium and resulting loss of potassium resulted in oxidative stress to prostate cell lines and led to apoptosis[47]. The results of these studies suggest, with proper formulation development, monensin and by extension sodium ionophores are broadly effective against cancers ranging from leukemia to glioblastomas to prostate lines. Additionally, these formulations have the potential to enhance the effect of drugs against resistant tumors.

Potassium

Many of the same applications that have proved successful for sodium delivery have analogs in the delivery of potassium. Unlike sodium, potassium has significantly higher concentrations within cell than in the serum. It is this potassium homeostasis that gives cells their average membrane potential of ~-90 mV[48]. The maintenance of this membrane potential is critical to the function of excitable cells such as neurons in the central nervous system and myocytes of the muscles. Interestingly, the natural ratio of intracellular to extracellular potassium seems to be more critical than the actual concentration[49-51]. In gradual elevation or depression of serum potassium levels, cells are able to adjust intracellular concentration to maintain the ratio needed for optimal membrane potential[52].

As with sodium delivery based on ionophores, potassium binding ionophores were first used as feed additives in poultry and ruminants[53,54]. Of the potassium ionophores used for this purpose, salinomycin and valinomycin have been the most extensively studied.

Potassium delivery to cancer cell lines, either as the main goal or as a sensitization technique, was relatively less studied compared to sodium delivery until recently. Valinomycin was the main potassium ionophore used for the initial studies. Initially it was found to display anti-tumor effects both in vitro and in vivo. To give the drug a longer lifetime and lower toxicity profile in vivo it was incorporated into liposomes[55]. This formulation led to reduced valinomycin toxicity in vivo by more than 10 fold. In tumor bearing animals the free drug led to no increase in survival time, but

the liposomal formulation resulted in a 40% increase [56]. As with monensin, valinomycin liposomes displayed synergistic effects when the injected with a traditional chemotherapeutic[57-59].

Interest in ionophore-based treatments for cancer was renewed in 2009 with the discovery that of 16,000 compounds tested, salinomycin was the most effective at inhibiting the growth and number of breast-cancer stem cells. This inhibition resulted in limited growth of treated tumors and a greatly reduced propensity for metastasis when compared to controls and paclitaxel **Figure 1.2**[60].

4T1 lung metastasis assay

Vehicle	Paclitaxel	Salinomycin
	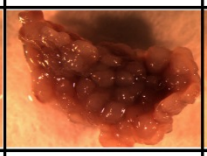	
1.38 ± 0.4	3.25 ± 0.21	0.36 ± 0.04

Figure 1.2 Tumor surface area and number of metastasis sites are significantly decreased by salinomycin treatment[60].

In addition to high toxicity to cancer stem cells, salinomycin was found to induce cell death in apoptosis resistant cell lines Jurkat CD4+ T-cell leukemia, Namalwa Burkitt lymphoma, and MES-SA/Dx5. Notably, the mechanisms of apoptosis and drug resistance are different for each of the three lines, overexpression of BcL-2, 26S proteasomes, and mdr-1 encoded P-glycoprotein respectively[61]. Another study found salinomycin is able to overcome resistance due to ATP-binding cassette transporters and does not induce resistance, even after 12 weeks[62]. These promising factors led to FDA approval of clinical testing of salinomycin in 2010. In two human cases that were

not responsive to traditional radiotherapy or chemotherapy, salinomycin was found to halt the progression of breast cancer and even reduce tumor volumes[63].

Chloride

In comparison to the extensive efforts spent on delivery of the other main biological monovalent ions, sodium and potassium, there has been relatively less focus on chloride. However, the large number of diseases that are due to endogenous chloride dysfunction has spurned efforts to better understand the movement and delivery of this ion[8]. The most well-known and characterized of these diseases is cystic fibrosis. In the disease a gene that controls certain chloride channels is defective and leads to reduced chloride transport in the lungs and intestines[64]. The lower chloride levels increases intracellular sodium concentrations requiring additional intracellular water. This depletes the available water for mucosal linings and increases their viscosity. Ultimately, the increased viscosity of the mucus leads to greater numbers of bacterial infections. The chronic, genetic nature of cystic fibrosis and multi-organ location suggests the greatest therapeutic benefits would be found in gene therapy rather than introduction of ionophores for chlorine.

However, in cancers, chloride transport is known to be significantly altered which leads to resistance to apoptosis and enhanced migration[9,65]. Though several chloride anion transporters have been synthesized, few have been thoroughly evaluated in biological systems[66,67]. Among the most extensively analyzed transporters, one group found that pyridine diamide-strapped calixpyrroles were able to effectively induce apoptosis by introduction of chlorine[67]. As with ionophores of sodium and potassium, decreased mitochondrial membrane potential and increased intracellular ROS

generation was indicated to be the main cause of toxicity. A follow-up study by the same group demonstrated that a number of synthesized aminopyrrolic compounds were able to inhibit the growth of both methicillin susceptible and methicillin resistant *S. aureus*[68]. This and the fact that these anion ionophores were mostly ineffective against gram negative bacteria suggest a similar mechanism to the previously discussed cation ionophores.

Lithium

As opposed to the previous three ions, lithium is naturally only present at trace amounts in humans with a total abundance of ~7mg, though this can vary widely based on Li^+ in the food and water supply[69]. In 1949, it was discovered that elevated levels of lithium could reduce the symptoms of mania and in 1974 the FDA approved its use for that purpose[70]. Even now, it is one of the frontline treatments for bipolar disorder. Though the benefits to treating mania and even alleviating some symptoms of depression were immediately discernable, the actual mechanism by which lithium operates was and continues to be a debated topic[71,72]. As a monovalent ion, it can possibly interact with many biological processes traditionally influenced by other charged species such as sodium, potassium, and magnesium. This broad potential activity and difficulty of experimentation on bipolar patients hinders research progress. Yet, over years of research, the two most commonly accepted mechanisms are the depletion of inositol and the inhibition of glycogen synthase kinase-3 (GSK-3)[73].

Abnormally high levels of the signaling potentiator inositol have been found in patients with bipolar disorder [74,75]. At elevated concentrations it forms a positive

feedback loop which supports synthesis of more inositol [73]. Lithium is an inhibitor of two enzymes that are needed for inositol metabolism, inositol monophosphatase and inositol polyphosphatase 1-phosphatase. This inhibition may stem from competitive binding between lithium and magnesium[76]. Another enzyme whose inhibition is modulated by this competition and whose dysregulation is associated with mental illnesses such as depression and bipolar disorder is glycogen synthase kinase-3[77-79]. This enzyme is a substrate for numerous cellular pathways including insulin signaling, neurotransmission, and inflammation response [80,81].

Most cells react to hazardous external stimuli by initiating inflammation. However, excessive and long-term inflammation has been linked to the pathogenesis of ailments such as cancer, depression, and osteoarthritis (OA)[82-84]. Due to its broad inhibitory effects lithium was recently suggested as a potential therapy for OA. Over the past six years a growing body of evidence has supported the claim that lithium can act as a means of treating the damage associated with osteoarthritis[85-88]. Recently, it was found that lithium reduces signaling of NF-κB and activation of p38 MAPK and STAT-3 which leads to lower expression of catabolic species that degrade cartilage[85,86]. Further work has suggested that lithium can inhibit Hedgehog signaling pathways by modulation of cilia on chondrocytes[87]. The reduction of these catabolic species in interleukin-1β (IL-1β) induced osteoarthritis models leads to protection of chondrocytes in vitro with a significant reduction in collagenolytic activity and collagen release **Figure 1.3**.

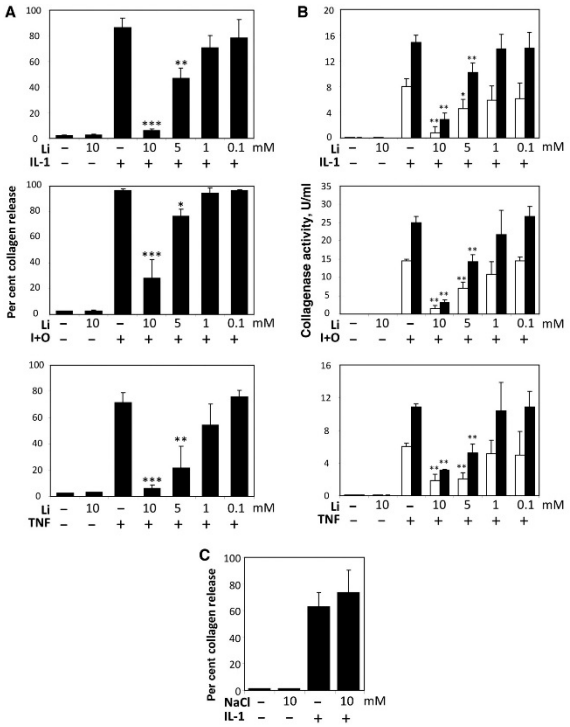

Figure 1.3 Collagen release (**A**) and collagenolytic activity (**B**) in cartilage stimulated by inflammatory cytokines. Sodium does not reduce collagen release (**C**)[85].

In vivo, lithium was found to minimize the loss of mechanical properties in excised rat joints and decrease Osteoarthritis Research Society International (OARSI) histologic scores in knee joints of mice[86,88]. In healthy joints, lithium displays no catabolic activity. In IL-1β induced models it completely protects against the degradation of cartilage stiffness and associated loss of mechanical properties **Figure 1.4**. The 50% decrease of OARSI scores further demonstrates the preservation of joint health using lithium therapy.

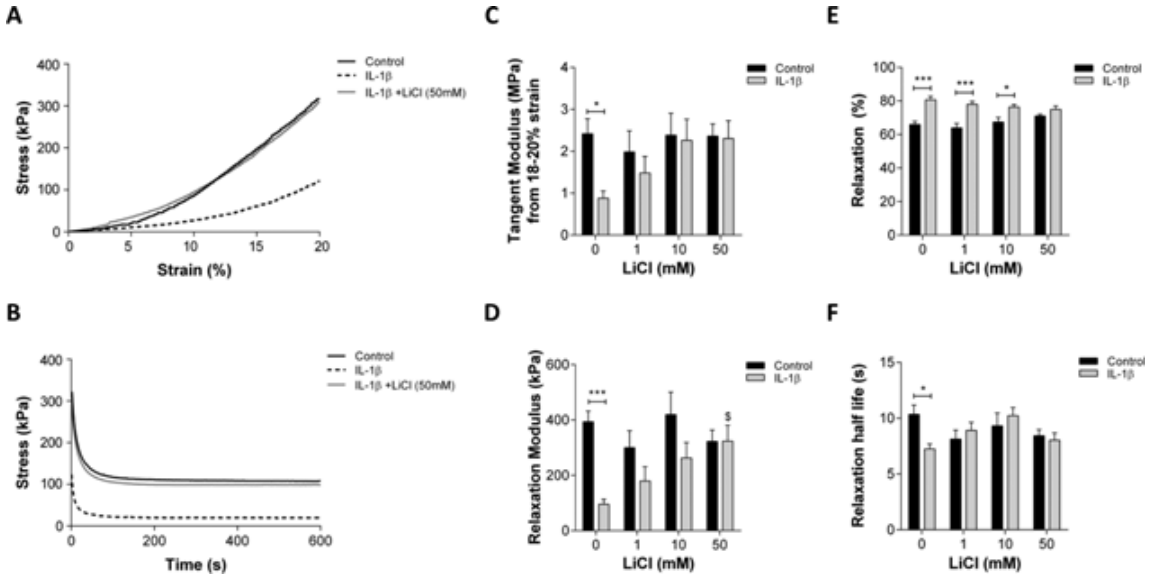

Figure 1.4 Lithium is able to completely inhibit the loss of cartilage mechanical properties

Nanoparticle Therapy

Nanomaterials have been extensively investigated as vehicles for drug delivery in cancer, vaccines, and arthritis[89-91]. The focal goal of nanoparticle drug delivery is increasing local concentrations of therapeutic agents in the disease site. Accomplishing this allows less active compound to be injected, reduces off-target toxicity, yields higher therapeutic efficacy, and extends therapy duration. To achieve these feats, many formulations have been investigated, some of which include: fullerenes, lipids, liposomes, polymers, silica, and gold. By their nature as nanoparticles, these delivery systems have very high relative surface areas for physical adsorption of therapeutic moieties. Additionally, many of the mentioned particles can be internally loaded with drugs allowing for higher carrying capacity and freeing the surface to provide further

functionality. As an example, poly(lactic-co-glycolic acid) (PLGA) polymer nanoparticles have been shown to load doxorubicin and when coated with poloxamer 188 limit tumor growth[92]. PLGA and other biodegradable particles have found extensive success due to minimal concerns with immediate and long term toxicity[93]. Ameliorated toxicity is a main factor in translation to clinical use, especially for cancer and arthritis development where the patient is likely to need subsequent treatments.

Biodegradable particles have a long history in cancer treatment. The first FDA approved nanoparticle drug, Doxil, has been used in the clinic for more than 20 years for cancer therapy[94]. This PEGylated nanoliposome displays a long circulation half-life which allows high tumor delivery by the enhanced permeability and retention (EPR) effect. Discovered in the 1980s, the EPR effect is due to malformed vasculature in tumors which allows nanomaterials to exit the blood stream and suppressed lymphatic drainage which inhibits the removal of the deposited particles[95]. As the EPR effect is broadly applicable to nanomaterials (10-100nm), the successful translation of biodegradable Doxil spurned the development of other nanomaterials for cancer therapy[96]. The aforementioned PLGA particles have been one of the most heavily studied vehicles for this application[97]. Compared with Doxil, doxorubicin-loaded PLGA has demonstrated comparable efficacy in decreasing the growth of tumor cells, but with significantly reduced cardiotoxicity. More advanced PLGA formulations with surface expressing targeting ligands such as aptamers and the peptide Arg-Gly-Asp have an even higher therapeutic effect due to increased tumor uptake[98,99].

Arthritis is another disease where biodegradable particles may provide significant benefits. In osteoarthritis, current treatments only focus on alleviating symptomatic pain

of the disease and only provide limited therapy[89]. Because of the uninhibited progression of the disease; higher amounts, stronger drugs, and more invasive procedures are eventually required to treat the pain. Of these options, intra-articular (IA) injection directly into the joint is a commonly used method of drug administration. Compared to systemic delivery, IA delivery allows higher concentrations of the drug in the diseased area with minimal concerns for toxicity to the greater body[100]. However, the residence time of small molecule drugs and even larger proteins is limited in the joint space after IA injection[101]. Nanoparticles that slowly release drugs are one method of solving this issue. Many of the same formulations used in cancer have been adapted for use in osteoarthritis[102]. In a large animal test, a radiolabeled small molecule was IA injected either as a free molecule or in liposomes[103]. The small molecule was undetectable in the joint within three hours, but the nanoparticle formulation displayed a half-life of 134 hours. A study using modified PLGA particles delivering a protein inhibitor of cartilage degradation in OA demonstrated significant chondro-protective effects and a 90% reduction in loss of protein activity[104].

While the attributes of these biodegradable nanoparticles for cancer and OA are manifold, there exists certain downsides as well. Liposomes have significant stability, uniformity, and reproducibility concerns[105]. Biodegradable polymers are difficult to scale up to meet clinical needs, exhibit a burst release of drug(s), and usually display a low loading rate (~1% m/m)[106]. An ideal nanoparticle drug delivery system would be non-immunogenic, biodegradable, carry a high payload, and accumulate significantly in desired locations.

One hypothetical class of nanoparticle drugs that would meet several of the above criteria is alkali halide nanostructures. The three members of the alkali metals are either predominant ions in the body or are FDA approved therapeutics. Of the halides, chloride is also one of the most significant naturally occurring ions in life. Iodide containing molecules have seen extensive use in medical imaging and iodide is considered an essential micronutrient. All alkali halides have high solubilities in aqueous solutions (with the exception of LiF) meaning biodegradability is of minimal concern and systematic immune response is also not likely. As nanoparticles these drugs would be able to accumulate through the EPR effect or have extended release due to their relatively large sizes. Delivery of other drugs or dyes would likely require surface adsorption of the desired molecules at low loading rates. However, as the densest source of these ions (short of the pure elements), nanoparticles made from alkali halides would be the most efficient method of delivery for ion-based therapy. Despite the promise, difficulties in managing the solubility in synthesis, nevermind controlled release, have resulted in no reports of alkali halide nanoparticles for any biomedical applications.

Dissertation Focus and Outline

The bulk of this dissertation is a report on the development of ion delivery by alkali halide nanoparticles for tumor therapy and osteoarthritis treatment. Notably, the two alkali halide projects described within are the first reports of both alkali halide nanoparticles and direct ion delivery for biomedical applications. Chapter two will cover sodium chloride nanoparticles for tumor therapy from synthesis through detailed in vitro characterization to preliminary in vivo results. Chapter three focuses on the

development of lithium fluoride nanoparticles that are able to reduce the damage associated with osteoarthritis. Chapter four is a report on using diatoms loaded with iron-oxide nanoparticles to provide magnetic targeting in tumor models. Lastly, chapter five will summarize the progress made in the separate projects and suggest further exploration in these new fields of nanomedicine.

References

(1) Milo, R.; Phillips, R.: *Cell biology by the numbers*. Garland Science p128-29

(2) Lang, F.; Waldegger, S. *Am Sci* **1997**, *85*, 456-463.

(3) Schultz, S. G.; Curran, P. F. *Physiol Rev* **1970**, *50*, 637-&.

(4) Demaurex, N. *News Physiol Sci* **2002**, *17*, 1-5.

(5) Strange, K. *Adv Physiol Educ* **2004**, *28*, 155-159.

(6) Suhail, M. Na, *Journal of clinical medicine research* **2010**, *2*, 1-17.

(7) Rolfe, D. F. S.; Brown, G. C. *Physiol Rev* **1997**, *77*, 731-758.

(8) Puljak, L.; Kilic, G. *Bba-Mol Basis Dis* **2006**, *1762*, 404-413.

(9) Cuddapah, V. A.; Sontheimer, H. (vol 301, pg C541, 2011). *Am J Physiol-Cell Ph* **2011**, *301*, C1479-C1479.

(10) Strobel, H. J.; Russell, J. B. *Appl Environ Microb* **1989**, *55*, 2664-2668.

(11) Huczynski, A. *Bioorg Med Chem Lett* **2012**, *22*, 7002-7010.

(12) *Feed Additive Compendium*; Miller Publishing: Minnetonka, MN, 1998.

(13) Raimondo, J. V.; Burman, R. J.; Katz, A. A.; Akerman, C. J. *Front Cell Neurosci* **2015**, *9*.

(14) Vanwinkle, L. J.; Christensen, H. N.; Campione, A. L. *Journal of Biological Chemistry* **1985**, *260*, 2118-2123.

(15) Broer, S. *Physiol Rev* **2008**, *88*, 249-286.

(16) Pittman, J. K. *Front Plant Sci* **2012**, *3*.

(17) Catterall, W. A. *Neuron* **2000**, *26*, 13-25.

(18) Keating, M. T.; Sanguinetti, M. C. *Cell* **2001**, *104*, 569-580.

(19) Graf, J.; Haussinger, D. *J Hepatol* **1996**, *24*, 53-77.

(20) Lamond, A. I. *Nature* **2002**, *417*, 383-383.

(21) Nature reviews. Molecular cell biology. Nature Pub. Group: London, UK, 2000; pp volumes.

(22) Gadsby, D. C. *Nat Rev Mol Cell Bio* **2009**, *10*, 344-352.

(23) Castillo, J. P.; Rui, H.; Basilio, D.; Das, A.; Roux, B.; Latorre, R.; Bezanilla, F.; Holmgren, M. *Nat Commun* **2015**, *6*.

(24) Workman, A. J.; Kane, K. A.; Rankin, A. C. *Cardiovasc Res* **2003**, *59*, 593-602.

(25) Magyar, C. E.; Wang, J.; Azuma, K. K.; McDonough, A. A. *Am J Physiol* **1995**, *269*, C675-682.

(26) Neuwinger, H. D.: *African ethnobotany : poisons and drugs : chemistry, pharmacology, toxicology*; Chapman & Hall: London ; New York, 1996.

(27) Dutton, C. J.; Banks, B. J.; Cooper, C. B. *Nat Prod Rep* **1995**, *12*, 165-181.

(28) Comben, N. *The Veterinary record* **1984**, *114*, 128.

(29) Russell, J. B.; Houlihan, A. J. *Fems Microbiol Rev* **2003**, *27*, 65-74.

(30) Clardy, J.; Walsh, C. *Nature* **2004**, *432*, 829-837.

(31) Bergen, W. G.; Bates, D. B. *Journal of animal science* **1984**, *58*, 1465-1483.

(32) Russell, J. B.; Strobel, H. J. *Appl Environ Microb* **1989**, *55*, 1-6.

(33) Dinius, D. A.; Simpson, M. E.; Marsh, P. B. *Journal of animal science* **1976**, *42*, 229-234.

(34) Dellinger, C. A.; Ferry, J. G. *Appl Environ Microb* **1984**, *48*, 680-682.

(35) Czerkaws.Jw; Harfoot, C. G.; Breckenr.G. *J Appl Bacteriol* **1972**, *35*, 537-551.

(36) Krause, D. O.; Russell, J. B. *Appl Environ Microb* **1996**, *62*, 815-821.

(37) Callaway, T. R.; Russell, J. B. *Curr Microbiol* **2000**, *40*, 185-189.

(38) Yang, C. M. J.; Russell, J. B. *Journal of animal science* **1993**, *71*, 3470-3476.

(39) Russell, J. B. *Journal of animal science* **1987**, *64*, 1519-1525.

(40) Booser, D. J.; Hortobagyi, G. N. *Drugs* **1994**, *47*, 223-258.

(41) Park, W. H.; Lee, M. S.; Park, K.; Kim, E. S.; Kim, B. K.; Lee, Y. Y. *Int J Cancer* **2002**, *101*, 235-242.

(42) Griffin, T.; Raso, V. *Cancer Res* **1991**, *51*, 4316-4322.

(43) van Horssen, P. J.; van Oosterhout, Y. V. J. M.; Evers, S.; Backus, H. H. J.; van Oijen, M. G. C. T.; Bongaerts, R.; de Witte, T.; Preijers, F. W. M. B. *Leukemia* **1999**, *13*, 241-249.

(44) Shaik, M. S.; Ikediobi, O.; Turnage, V. D.; McSween, J.; Kanikkannan, N.; Singh, M. *J Pharm Pharmacol* **2001**, *53*, 617-627.

(45) Shaik, M. S.; Jackson, T. L.; Singh, M. *J Pharm Pharmacol* **2003**, *55*, 819-825.

(46) Iljin, K.; Ketola, K.; Vainio, P.; Halonen, P.; Kohonen, P.; Fey, V.; Grafstrom, R. C.; Perala, M.; Kallioniemi, O. *Clin Cancer Res* **2009**, *15*, 6070-6078.

(47) Ketola, K.; Vainio, P.; Fey, V.; Kallioniemi, O.; Iljin, K. *Mol Cancer Ther* **2010**, *9*, 3175-3185.

(48) Tetzlaff, J. E.; Ohara, J. F.; Walsh, M. T. *Can J Anaesth* **1993**, *40*, 227-246.

(49) Barold, S. S.; Falkoff, M. D.; Ong, L. S.; Heinle, R. A. *J Am Coll Cardiol* **1987**, *10*, 467-469.

(50) Lubbe, W. F.; Holland, R. K.; Gilchrist, A. I.; Pybus, J. *J Mol Cell Cardiol* **1986**, *18*, 37-41.

(51) Macconaill, M. *Cardiovasc Res* **1987**, *21*, 463-468.

(52) Wright, F. S.; Giebisch, G. *Am J Physiol* **1978**, *235*, F515-F727.

(53) Daugschies, A.; Gasslein, U.; Rommel, M. *Vet Parasitol* **1998**, *76*, 163-171.

(54) Callaway, T. R.; Edrington, T. S.; Rychlik, J. L.; Genovese, K. J.; Poole, T. L.; Jung, Y. S.; Bischoff, K. M.; Anderson, R. C.; Nisbet, D. J. *Current issues in intestinal microbiology* **2003**, *4*, 43-51.

(55) Daoud, S. S.; Juliano, R. L. *Cancer Res* **1986**, *46*, 5518-5523.

(56) Daoud, S. S.; Juliano, R. L. *P Am Assoc Canc Res* **1986**, *27*, 409-409.

(57) Daoud, S. S.; Forde, N. H. *Cancer Chemoth Pharm* **1991**, *28*, 370-376.

(58) Crifo, C.; Capuozzo, E.; Cucco, C.; Zupi, G.; Salerno, C. *Biochem Int* **1991**, *25*, 593-601.

(59) Daoud, S. S.; Juliano, R. L. *Cancer Res* **1989**, *49*, 2661-2667.

(60) Gupta, P. B.; Onder, T. T.; Jiang, G. Z.; Tao, K.; Kuperwasser, C.; Weinberg, R. A.; Lander, E. S. *Cell* **2009**, *138*, 645-659.

(61) Fuchs, D.; Heinold, A.; Opelz, G.; Daniel, V.; Naujokat, C. *Biochemical and biophysical research communications* **2009**, *390*, 743-749.

(62) Fuchs, D.; Daniel, V.; Sadeghi, M.; Opelz, G.; Naujokat, C. *Biochemical and biophysical research communications* **2010**, *394*, 1098-1104.

(63) Naujokat, C.; Steinhart, R. *J Biomed Biotechnol* **2012**.

(64) Riordan, J. R.; Rommens, J. M.; Kerem, B. S.; Alon, N.; Rozmahel, R.; Grzelczak, Z.; Zielenski, J.; Lok, S.; Plavsic, N.; Chou, J. L.; Drumm, M. L.; Iannuzzi, M. C.; Collins, F. S.; Tsui, L. C. *Science* **1989**, *245*, 1066-1072.

(65) Lehen'kyi, V.; Shapovalov, G.; Skryma, R.; Prevarskaya, N. *Am J Physiol-Cell Ph* **2011**, *301*, C1281-C1289.

(66) Moore, S. J.; Wenzel, M.; Light, M. E.; Morley, R.; Bradberry, S. J.; Gomez-Iglesias, P.; Soto-Cerrato, V.; Perez-Tomas, R.; Gale, P. A. *Chem Sci* **2012**, *3*, 2501-2509.

(67) Ko, S. K.; Kim, S. K.; Share, A.; Lynch, V. M.; Park, J.; Namkung, W.; Van Rossom, W.; Busschaert, N.; Gale, P. A.; Sessler, J. L.; Shin, I. *Nat Chem* **2014**, *6*, 885-892.

(68) Share, A. I.; Patel, K.; Nativi, C.; Cho, E. J.; Francesconi, O.; Busschaert, N.; Gale, P. A.; Roelens, S.; Sessler, J. L. *Chemical communications* **2016**, *52*, 7560-7563.

(69) Aral, H.; Vecchio-Sadus, A. *Ecotox Environ Safe* **2008**, *70*, 349-356.

(70) Shorter, E. *Bipolar Disord* **2009**, *11*, 4-9.

(71) Marmol, F. Lithium: *Prog Neuro-Psychoph* **2008**, *32*, 1761-1771.

(72) Coppen, A. *The Journal of clinical psychiatry* **2000**, *61 Suppl 9*, 52-56.

(73) Brown, K. M.; Tracy, D. K. *Therapeutic advances in psychopharmacology* **2013**, *3*, 163-176.

(74) Silverstone, P. H.; McGrath, B. M.; Kim, H. *Bipolar Disord* **2005**, *7*, 1-10.

(75) Allison, J. H.; Stewart, M. A. *Nature: New biology* **1971**, *233*, 267-268.

(76) Dudev, T.; Lim, C. *J Am Chem Soc* **2011**, *133*, 9506-9515.

(77) Polter, A.; Beurel, E.; Yang, S. F.; Garner, R.; Song, L.; Miller, C. A.; Sweatt, J. D.; McMahon, L.; Bartolucci, A. A.; Li, X. H.; Jope, R. S. *Neuropsychopharmacology : official publication of the American College of Neuropsychopharmacology* **2010**, *35*, 1761-1774.

(78) Inkster, B.; Nichols, T. E.; Saemann, P. G.; Auer, D. P.; Holsboer, F.; Muglia, P.; Matthews, P. M. *Arch Gen Psychiat* **2009**, *66*, 721-728.

(79) Ryves, W. J.; Harwood, A. J. *Biochemical and biophysical research communications* **2001**, *280*, 720-725.

(80) Kaidanovich-Beilin, O.; Woodgett, J. R. *Front Mol Neurosci* **2011**, *4*.

(81) Klein, P. S.; Melton, D. A. A molecular mechanism for the effect of lithium on development. *P Natl Acad Sci USA* **1996**, *93*, 8455-8459.

(82) Coussens, L. M.; Werb, Z. *Nature* **2002**, *420*, 860-867.

(83) Miller, A. H.; Raison, C. L. *Nat Rev Immunol* **2016**, *16*, 22-34.

(84) Sokolove, J.; Lepus, C. M. *Therapeutic advances in musculoskeletal disease* **2013**, *5*, 77-94.

(85) Hui, W.; Litherland, G. J.; Jefferson, M.; Barter, M. J.; Elias, M. S.; Cawston, T. E.; Rowan, A. D.; Young, D. A. *Rheumatology* **2010**, *49*, 2043-2053.

(86) Minashima, T.; Zhang, Y.; Lee, Y.; Kirsch, T. *Arthritis Rheumatol* **2014**, *66*, 1228-1236.

(87) Thompson, C. L.; Wiles, A.; Poole, C. A.; Knight, M. M. *Faseb J* **2016**, *30*, 716-726.

(88) Thompson, C. L.; Yasmin, H.; Varone, A.; Wiles, A.; Poole, C. A.; Knight, M. M. *J Orthop Res* **2015**, *33*, 1552-1559.

(89) Periyasamy, P. C.; Leijten, J. C. H.; Dijkstra, P. J.; Karperien, M.; Post, J. N. *J Nanomater* **2012**.

(90) Gregory, A. E.; Titball, R.; Williamson, D. *Front Cell Infect Mi* **2013**, *3*.

(91) Chen, H. M.; Zhen, Z. P.; Todd, T.; Chu, P. K.; Xie, J. *Mat Sci Eng R* **2013**, *74*, 35-69.

(92) Wohlfart, S.; Khalansky, A. S.; Gelperina, S.; Maksimenko, O.; Bernreuther, C.; Glatzel, M.; Kreuter, J. *Plos One* **2011**, *6*.

(93) Kumari, A.; Yadav, S. K.; Yadav, S. C. Biodegradable polymeric nanoparticles based drug delivery systems. *Colloid Surface B* **2010**, *75*, 1-18.

(94) Barenholz, Y. Doxil (R) - *J Control Release* **2012**, *160*, 117-134.

(95) Maeda, H.; Wu, J.; Sawa, T.; Matsumura, Y.; Hori, K. *J Control Release* **2000**, *65*, 271-284.

(96) Kobayashi, H.; Watanabe, R.; Choyke, P. L. *Theranostics* **2014**, *4*, 81-89.

(97) Park, J.; Fong, P. M.; Lu, J.; Russell, K. S.; Booth, C. J.; Saltzman, W. M.; Fahmy, T. M. *Nanomed-Nanotechnol* **2009**, *5*, 410-418.

(98) Guo, J. W.; Gao, X. L.; Su, L. N.; Xia, H. M.; Gu, G. Z.; Pang, Z. Q.; Jiang, X. G.; Yao, L.; Chen, J.; Chen, H. Z. *Biomaterials* **2011**, *32*, 8010-8020.

(99) Danhier, F.; Vroman, B.; Lecouturier, N.; Crokart, N.; Pourcelle, V.; Freichels, H.; Jerome, C.; Marchand-Brynaert, J.; Feron, O.; Preat, V. *J Control Release* **2009**, *140*, 166-173.

(100) Holyoak, D. T.; Tian, Y. F.; van der Meulen, M. C. H.; Singh, A. *Ann Biomed Eng* **2016**, *44*, 2062-2075.

(101) Coleman, P. J.; Scott, D.; Ray, J.; Mason, R. M.; Levick, J. R. *J Physiol-London* **1997**, *503*, 645-656.

(102) Morgen, M.; Tung, D.; Boras, B.; Miller, W.; Malfait, A. M.; Tortorella, M. *Pharm Res-Dordr* **2013**, *30*, 257-268.

(103) Edwards, S. H. R.; Cake, M. A.; Spoelstra, G.; Read, R. A. *J Liposome Res* **2007**, *17*, 249-261.

(104) Whitmire, R. E.; Wilson, D. S.; Singh, A.; Levenston, M. E.; Murthy, N.; Garcia, A. J. *Biomaterials* **2012**, *33*, 7665-7675.

(105) Immordino, M. L.; Dosio, F.; Cattel, L. *Int J Nanomed* **2006**, *1*, 297-315.

(106) Danhier, F.; Ansorena, E.; Silva, J. M.; Coco, R.; Le Breton, A.; Preat, V. *J Control Release* **2012**, *161*, 505-522.

CHAPTER 2

KILLING CANCER WITH SALT: DIRECT INTRACELLULAR ION DELIVERY USING SODIUM CHLORIDE NANOPARTICLES

Todd, T.; Chen, H.; Zhou, S.; Yin, L.; Yu, X.; Xie, J. To be submitted to *Nature*

Abstract

Sodium chloride has been known to humans for millennia as a flavor enhancer. Biologically, its two constituent ions are among the most prevalent and important ions for healthy cellular function. The highly controlled balance of these ions across cell membranes is critical to cellular volume, signaling, transport, and electrical excitation. Molecules that shuttle sodium and chloride through the cell membrane and thereby disrupt the natural ion gradient are broadly toxic to cells. We have synthesized sodium chloride nanoparticles for direct ion delivery to the intracellular environment. The particles display toxicity in a dosage dependent manner when immediately reconstituted and injected. However, the particles degrade into harmless sodium and chloride ions in aqueous environments allowing modulation of therapeutic effect and ameliorating concerns of long-term toxicity. A proof-of-concept study in immunocompetent breast cancer model animals found the particles were able to decrease the relative growth of tumors by 2-3 fold.

Introduction

The balance of ion concentrations across the cell membrane is one of the most critical aspects to maintaining healthy cellular function. All healthy animal cells sustain high ratios of intracellular to extracellular potassium, and low ratios of sodium, chloride, and calcium[1]. It is these asymmetric ion concentrations that drive numerous cell processes including transport of amino acids across the cell membrane[2,3], maintenance of cellular pH[4,5], control of cell volume[6,7], and generation of electrical impulses in excitable cells[8,9]. Because the cell membrane is effectively impermeable to charged species, specialized protein pumps are required to ensure healthy ion levels in the intra-

and extracellular spaces[10]. Of these pumps, Na^+/K^+ ATPase is one of the most studied and important because of its central role in creating the homeostasis of potassium and sodium[11]. This pump expels three sodium ions from the cell and transports two potassium ions into the cell, consuming one molecule of ATP in the process. Unsurprisingly, inhibitors of Na^+/K^+ ATPase disrupt ion homeostasis and lead to cell death[12]. Rather than disabling endogenous pumps, certain molecules can circumvent natural ion regulators completely by transporting ions directly across the cell membrane.

These molecules, called ionophores, chelate and encapsulate charged species, shuttling them with the inherent concentration gradient thereby eroding the asymmetric ion concentrations[13]. As with ion pump inhibition, ionophore-based disruption of natural potassium and sodium gradients leads to toxicity. Because of this, these molecules have been used for decades in ruminant and poultry feedstock as antibiotics[13,14]. In gram positive bacteria they lead to cell death by depletion of ATP, osmotic collapse, and excessive secondary ion pump activation[15-18]. Recent research has suggested ionophores as effective drugs for cancer therapy. The sodium ionophore monensin was found to selectively inhibit growth of prostate cancer cells while causing minimal damage to primary cell lines[19]. Salinomycin, a potassium ionophore, has demonstrated the ability to kill cancer stem cells in breast cancer lines[20]. It has also been found to overcome apoptosis and drug resistance in Jurkat CD4+ T-cell leukemia, Namalwa Burkitt lymphoma, and MES-SA/Dx5 uterine sarcoma[21]. Notably, each cell line displays a different resistance mechanism. Despite the promising results, the inherent lipophilicity and potential off target toxicity of ionophores has limited their translation into the clinic[22,23].

Herein, we report a novel method of anti-tumor therapy based upon the transfer of high amounts of sodium and chloride ions across the cell membrane. This is achieved by newly synthesized sodium chloride nanoparticles. These particles maintain limited aqueous stability due to their phospholipid coating allowing them to remain intact as they traverse the cell membrane. Once internalized, degradation of the particles allows rapid release of constituent ions, damaging the ionic balance of cells sufficiently to induce necrosis. This form of cell death has not been reported in therapeutics that disrupt the asymmetric ion gradient in cells. The effect of this delivery system is demonstrated in a proof-of-concept study where 4T1 breast cancer models were intratumorally injected with nanoparticles. Tumor growth was significantly inhibited by injection of nanoparticles, but not by equal molar aqueous sodium chloride. To the best of our knowledge, direct delivery of ions into cells for therapeutic purposes has never been reported in the literature. This report demonstrates the feasibility of nanoparticle-mediated ion delivery and suggests the benefits of exploring alkali halide nanoparticles as delivery vehicles.

Hypothesis

We hypothesize that directly delivering high concentrations of sodium chloride into cells independent of ion pumps or shuttling molecules would disturb the natural ion homeostasis and lead to cellular damage and death. While sodium and chloride are present at high concentrations in extracellular spaces, because ions cannot move across the cell membrane the endogenous ion pumps can maintain a healthy balance. Nanoparticle uptake, as a means of drug delivery, bypasses the membrane and can introduce relatively large quantities of therapeutic species rapidly into the cell.

Delivering a single 100 nm sodium chloride nanoparticle into the cytoplasm introduces more than 22 million sodium and chloride ions. We believed utilizing sodium chloride nanoparticles (NaCl NPs) can achieve this ion delivery **Figure 2.1**. Temporarily stable NaCl NPs will be internalized by cells and quickly broken down into constituent ions. The increase in intracellular ions disrupts several pathways and eventually causes cell death. Notably, nanoparticles that dissolve in the serum will pose no toxicity to cells as the active 'drugs' will become part of the body's sodium and chloride stores. Within 12 hours all particles are dissolved ameliorating any remaining concerns for long term toxicity.

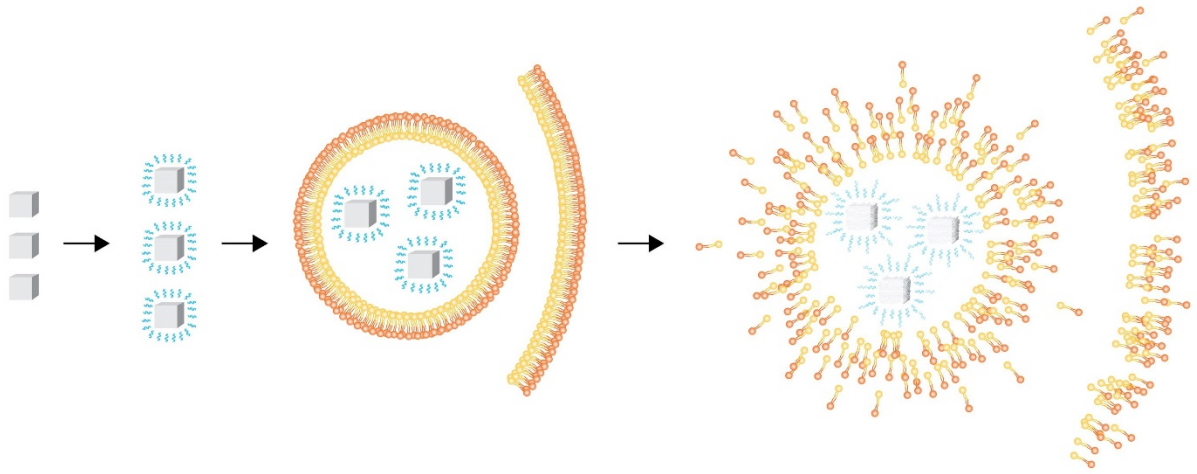

Figure 2.1 Schematic representation of NaCl NP therapy. Particles are synthesized, then coated with phospholipid to endow them with limited aqueous stability. The particles are added to cells where they are internalized and then degrade releasing high amounts of Na^+ and Cl^- killing the cell.

Materials and Methods

Synthesis of NaCl NPs

Approach 1. 0.2 mmol (0.0608 g) of sodium oleate (Sigma) is added to 10 mL of 1-octadecene and heated at 200°C until the solid is dissolved. The solution is allowed to cool to room temperature. 1 mL oleylamine and then 0.15 mmol of molybdenum(V)chloride (Sigma) is added to the solution, the vial is capped, and the reaction is allowed to proceed overnight. The particles are purified by centrifugation at 9000rpm (9682 rcf) for 10 minutes, decanting the supernatant, and then dispersing the particles in hexanes using brief sonication. This process is repeated 3x to ensure the removal of unreacted species. After the last dispersal in 10mL hexane, the particles are again sonicated and remain stable in solution at 4°C for a week.

Approach 2. 1.0 mmol (0.230g) of 1,2-tetradecanediol(Sigma) is added to 3.04 mmol (1.00mL) oleylamine (Sigma) and 9 mL hexanes in a 15 mL vial with a stir bar. While stirring, the vial is heated until the 1,2-tetradecanediol is dissolved and the subsequent solution is allowed to cool to room temperature. 0.15 mmol (0.0400g) molybdenum(V)chloride (Sigma) is added to the solution, the vial is capped, and the reaction is allowed to proceed overnight. The particles are purified using the same protocol as approach1.

Coating of NaCl NPs with phospholipid and dispersal in PBS

The freshly synthesized or stored particles are sonicated for 20-30 seconds to ensure their full dispersity in solution. 80 µL of 1 mg/mL (total phospholipid added is 80µg or 2.87×10^{-8} mol) 1,2-distearoyl-*sn*-glycero-3-phosphoethanolamine-N-

[amino(polyethylene glycol)-2000] (ammonium salt) (Avanti Polar Lipids) in chloroform is added to the NaCl NP solution and allowed to sonicate for ~30 seconds. The resulting solution is added to a round bottom flask and the solvent is evaporated under reduced pressure in a Buchi R II Rotavapor with the water bath set to 40°C. The particles are allowed to dry for 30 minutes and are then removed for either immediate testing or sealed with parafilm with an argon atmosphere and stored at 4°C or -20°C for up to 1 week. When the dried particles are needed, 10 mL of PBS solution is added to the flask and sonicated for 30-60 seconds. The resulting solution is introduced to cells or animals immediately to ensure high therapeutic effect.

Cellular studies

PC-3 (human prostate cancer) cells (ATCC) were grown in RPMI1640 medium supplemented with 10% FBS and 100 units/mL of penicillin and 100 units/mL streptomycin (MediaTech, USA). The cells were maintained in a humidified, 5% carbon dioxide atmosphere at 37 °C. For cellular studies, 10^4 PC-3 cells were seeded in 96-well plates (Corning) and cultured for 24 h.

Microscope Studies

The time dependent live/dead, mitochondria tracking, nanoparticle uptake, and ion quantification assays were carried out on a Cellomics® ArrayScan® VTI HCS Reader with a live cell chamber and HCS Studio™ 2.0 Cell Analysis Software (Thermo Scientific). 36 fields per well were acquired using a 20 x objective (NA 0.5), a Hamamatsu ORCA-ER digital camera in combination with a 0.63x coupler and Carl

Zeiss microscope optics in auto focus and high resolution mode. In the two or three dye assays channel one uses the BGRFR 386-23 filter for Hoechst 33342(nuclei) and is. Channel one is also used for auto-focus, object identification, and segmentation. Image smoothing was applied to reduce object fragmentation prior to object detection. Channel two uses BGRFR 485-20 filter for SBFI, PBFI, MQAE, calcien AM dye, or mitochondria. Finally, channel three applies BGRFR 549-15 and images ethidium homodimer-III or rhodamine B.

All cells were identified in channel one (Ch1) using a nuclear stain Hoechst 33342, and cell features included cell number, nuclear area, and nuclear shape measurement: P2A and LWR, total, average and variance intensities for each channel. NucShapeP2A indicated nucleus smoothness based on ratio of perimeter squared to 4π*nucleus area of Ch1 nucleus, while NucShapeLWR indicated nuclear roundness based on ratio of length to width. Total intensity was defined as total intensity of all pixels within respective channel. Average Intensity was defined as average intensity of all pixels within respective channel. At least 5000 cells were included in each well.

Characterization of NaCl Nanoparticles

TEM samples were prepared by depositing 2.5 µL of sample onto formvar-coated copper grids(Electron Microscopy Sciences) and drying under reduced pressure for at least 6 hours. NaCl particles were imaged using a FEI Tecnai 20 transmission electron microscope operating at 200kV. 20µL samples were dried on silicon wafers for SEM and EDS testing. SEM and elemental mapping images were acquired on a FEI Teneo

field emission scanning electron microscope equipped with an Oxford EDS system. X-ray diffraction analysis was carried out on a Bruker D8-Advance using dried sample on a cut glass slide.

Cytotoxicity test

The 3-(4, 5)-dimethylthiahiazo (-z-y1)-3, 5-di-phenytetrazolium-romide (MTT, Gibco) method was used to study the cytotoxicity of NaCl NPs on PC-3 cells and determine optimal concentrations for further testing. Cells seeded in 96 well-plates were treated with NaCl at various concentrations (2-125 µg/mL Na^+) for 24 hours. Then, 20 µL of 5 mg/mL MTT reagent was added in 200 µL of test culture medium and incubated at 37°C for 4 h. 200 µL of DMSO was added to dissolve the formazan product after the supernatant was removed. The absorbance was measured on a microplate reader (BioTeK, Synergy Mx) at 490 nm and the measurements were performed in sextuplicate.

Particle dissolution time dependent cytotoxicity

The change in cytotoxicity due to particle degradation was measured using the MTT test protocols described previously. NaCl NPs were added to cells (64 µg/mL Na^+) immediately after reconstitution in PBS (t=0), 1 hour after reconstitution, 3 hours, and 8 hours after. The MTT protocol was performed 24 hr after the last addition of particles.

Time dependent live/dead cell assay

The time dependent toxicity of the NaCl NPs was evaluated using the dyes Hoechst 33342, calcein-AM, and ethidium homodimer-III. Cells seeded in 96 well plates were treated with NaCl NPs (64 µg/mL Na^+), NaCl in PBS solution (64 µg/mL Na^+ added), and PBS. Solutions of the three dyes were added to each well to bring the

concentrations of Hoechst 3342, calcein AM, and ethidium homodimer-III to 8 µM, 5 µM, and 5 µM, respectively. The plates were imaged on the microscope system described above using channels 1, 2, and 3.

Mitochondria tracking

Location and expression of mitochondria relative to the nucleus was determined using MitoTracker® Green and Hoechst 33342. The dyes were loaded into individual wells to reach a final concentration of 100 nM and 8 µM for MitoTracker® and Hoechst, respectively. Imaging was carried out on the microscope system described above using channels 1 and 2.

Determination of apoptosis or necrosis cell death

Determination of cellular death pathway was carried out by an apoptotic, necrotic, and healthy cells quantification kit (Biotium, 30018). PC-3 cells were grown on tissue culture dishes (Corning, 35 mm x 10 mm) by addition of 5 x 10^4 cells and overnight incubation. NaCl nanoparticles (64 µg/mL Na^+) were added to the dishes. A working dye solution was made according to manufacture protocols by adding 100 µL of diluted binding buffer to 5 µL Hoechst 33342, 5 µL of FITC-Annexin V, and 5 µL ethidium homodimer-III. At 2, 4, and 6 hours after addition of NaCl NPs the cells were washed with PBS, and the working solution was incubated with the cells for 15 minutes. The cells were washed with binding buffer twice and then covered with more binding buffer for fluorescence imaging. Fluorescence images were acquired on a fluorescence microscope using the dapi channel for Hoechst 33342, the FITC channel for AnnexinV-FITC, and the TRITC channel for ethidium homodimer-III.

Sodium/potassium/chlorine intracellular concentrations and nanoparticle uptake

Time dependent ion concentration changes were analyzed by SBFI-AM, PBFI-AM, and MQAE(Setareh Biotech) dyes for sodium, potassium, and chlorine respectively. The sodium and potassium dyes were loaded by dissolving 50 µg of the dye in 11.09 µL of DMSO and 11.09 µL of Pluronic F-127 solution in DMSO (20% m/m). The solution is added to 4,414 µL of RPMI medium, mixed, and 100µL used to replace the growth medium in each well of a 96 well plate. A two hour incubation is followed by twice washing cells with PBS and immediate addition of the nanoparticle solution in FBS free medium. MQAE is added by dissolving 6.5 mg MQAE in two mL of FBS free medium and subsequent replacement of the growth medium with the MQAE medium for 2 hours. Nanoparticle uptake was determined by adding the fluorescent-labeled phospholipid, 1,2-dipalmitoyl-*sn*-glycero-3-phosphoethanolamine-N-(lissamine rhodamine B sulfonyl) (ammonium salt) (40 µL of 1 mg/ mL, Avanti Polar Lipids) to 40 µL of the amine terminated PEGylated phospholipid when coating the particles. Labeled nanoparticles were added to cells loaded with each of the dyes and Hoechst 33432(see live/dead assay for loading). Fluorescent measurements were taken at two hours.

Mitochondrial membrane potential

Mitochondrial membrane potential was measured using the JC-1 mitochondrial membrane potential detection kit (Biotium, 30001). The JC-1 working solution was prepared by adding 10 µL of the concentrated dye to 1 mL of FBS free RPMI medium. NaCl NPs (6, 10, 32, 64 µg/mL Na^+), PBS control, and aqueous NaCl control (64 µg/mL Na^+) were added to the cells. After 2 hours the medium was removed and replaced with

the JC-1 working solution. After a 15 minute incubation the cells were read on a microplate reader with excitation and emission wavelengths of 485/535 nm for the green, monomeric dye and 550/600 for the red, aggregated dye.

Animals

Balb/c mice were purchased from Harlan laboratories. The animal model was established by subcutaneously injecting ≈5 × 10^6 4T1 cells into the right hind limb of each mouse. All of the experimental procedures had been conducted following a protocol approved by the University of Georgia Institutional Animal Care and Use Committee.

Therapy Studies

Therapy studies were carried out on 4T1 tumor models. Five 4-6 week old Balb/c mice were subcutaneously injected with 5 × 10^6 4T1 cells into the right hind limb. The study started when the tumors reached a size of approximately 100mm^3(12 days after injection of cells). Three treatment animals were injected with 50µL of nanoparticle solution in PBS (313, 208, or 104 µg/mL Na^+ added). Control animals were injected with 50µL PBS or 50µL PBS with NaCl salt added (313µg/mL Na^+). Tumor sizes were measured using a caliper every two days. Tumor volume was calculated from the following equation: mm^3 = length (mm) × $width(mm)^2/2$.

Results

Sodium chloride nanoparticle synthesis, coating, and characterization

We developed two methods to synthesize sodium chloride nanoparticles. In the first approach we used sodium oleate and $MoCl_5$ as the sources for sodium and

chloride, respectively. The low solubility of oleate complexes makes removal of excess starting material difficult in this synthesis. We have also investigated a synthesis between of 1,2-tetradecanediol and $MoCl_5$ in hexane and oleylamine. Lack of a sodium source was puzzling, but ICP analysis showed that sodium is an approximately 1% by weight impurity in 1,2-tetradecanediol. The amount of sodium added in this approach is therefore similar to the amount used in oleate synthesis. The synthesized particles are cubic and have a size distribution of 50-100 nanometers in diameter from TEM analysis **Figure 2.3a**. XRD spectra and SEM-EDS elemental analysis confirm that the particles are made of sodium chloride **Figure 2.3(b-e)**. The particles are coated with an amine terminated and PEGylated phospholipid to endow the particles with aqueous stability **Figure 2.2**. This form of surface modification is extensively reported in literature[24]. The non-polar tails of the oleylamine nanoparticle coating and the phospholipid are bound together through hydrophobic-hydrophobic interations. This expresses the hydrophilic PEG 2000 linkage and the terminal amine to the aqueous environment.

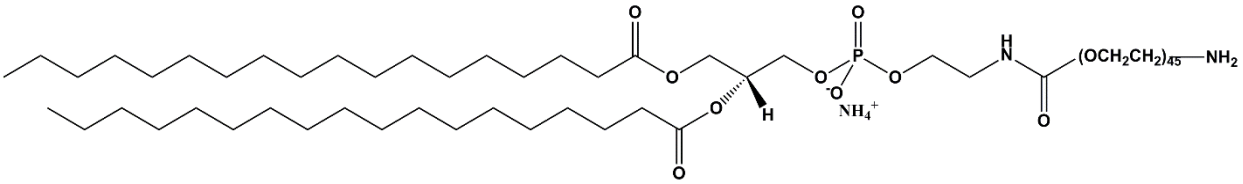

Figure 2.2 Molecular structure of the phospholipid used for coating

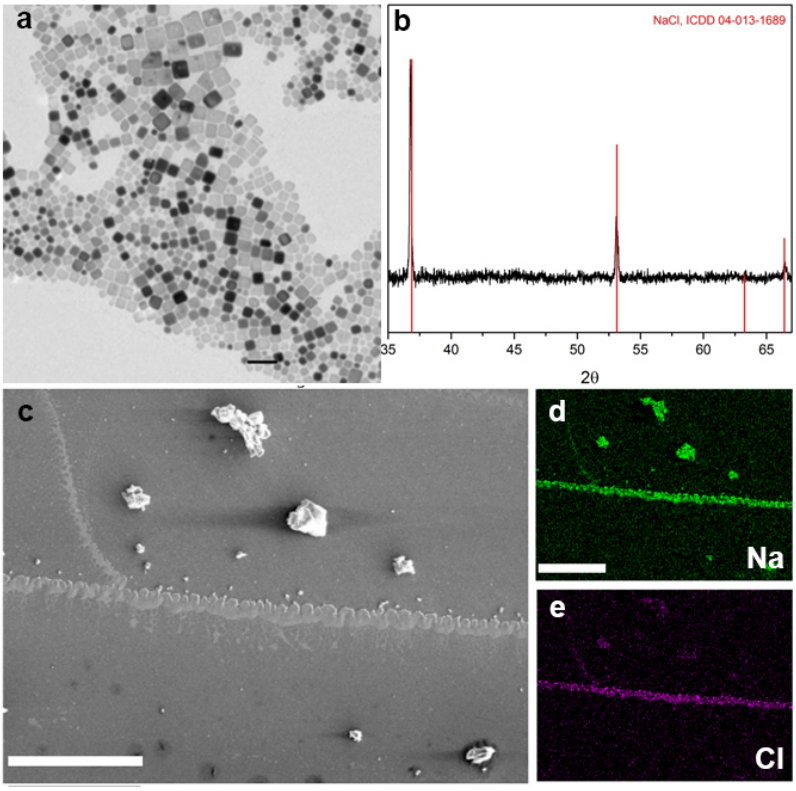

Figure 2.3 Characterization of NaCl nanoparticles (a) TEM image of NaCl nanoparticles, scale bar 100 nm. (b) XRD of NaCl particles. (c) SEM image of NaCl nanoparticles, scale bar 2.5 µm. (d,e) Elemental mapping of (c) for sodium and chlorine, (d) and (e) respectively. Scale bar 2.5 µm

Sodium chloride nanoparticles are toxic to cells, but the toxicity is dependent on the time the particles are dispersed in aqueous solution

Evaluation of viability using MTT assay was performed to determine acceptable concentrations of NaCl NPs for further use **Figure 2.4a**. The particles display a dose dependent toxicity with an IC50 value of ~64 µg/mL Na^+ added from the particles**.** This toxicity was also contingent on the length of time the particles had been dispersed in

aqueous solutions **Figure 2.5a**. Addition of the particles immediately after suspension in PBS resulted in the highest degree of toxicity. Addition of the particles after 1hr, 3hr, and 8 hrs in PBS resulted in increasing viability for each later time point.

Figure 2.4 Toxicity of NaCl NPs (a) MTT assay of NaCl NPs shows an IC_{50} value of ~64 µg/mL Na^+ added. (b) Live/dead assay of nanoparticles at different concentrations at 1,2,4, and 6 hours (µg/mL Na^+ added). Rapid increase of toxicity is seen between 4 and 6 hours.

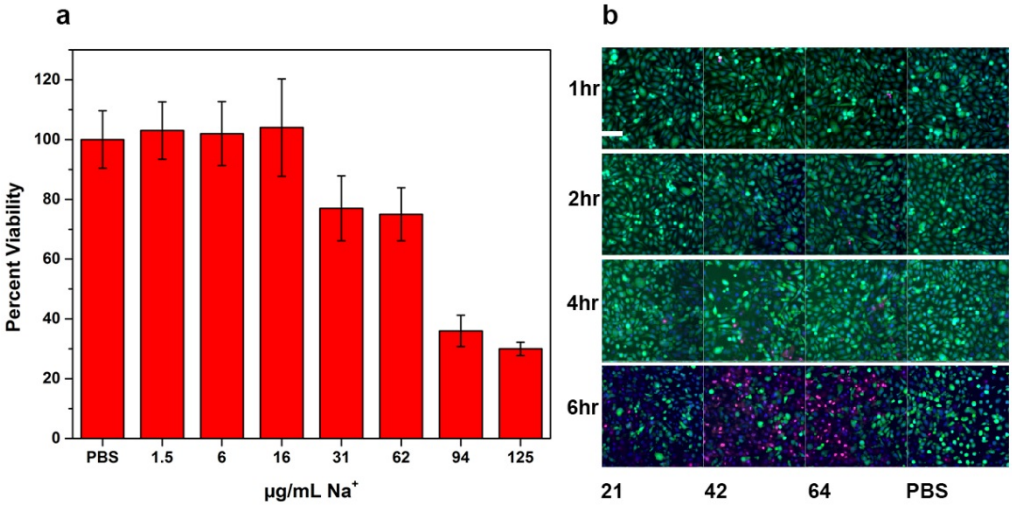

Sodium chloride nanoparticles display a rapid increase in toxicity between four and six hours

A live/dead fluorescence assay was used to determine the time point at which the cells were no longer viable **Figure 2.4b**. There are minimal changes in viability visible in the first two hours after particle addition, and a very small amount of positive dead staining at four hours. However, at six hours, there is a marked increase of cell

death and a significant decrease in the number of viable cells **Supporting Information Figure 2.11**.

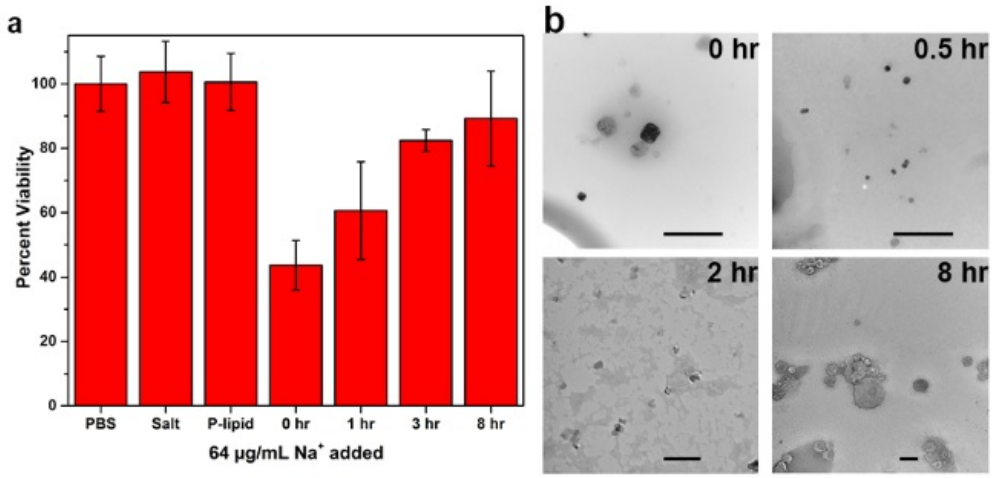

Figure 2.5 Dissolution of NaCl and Toxicity reduction (a) Toxicity of NaCl NPs after the indicated amounts of time in PBS. (b) TEM images of NaCl after the indicated amount of time in water. Scale bar 250 nm

Co-localization of sodium, potassium, and chlorine with nanoparticles

The delivery of sodium into cells from the particles was assessed using the fluorescent dyes SBFI-AM **Figure 2.6a**. The potassium dye PBFI-AM was used to measure the relative increase in potassium concentration **Figure 2.6b**. An increase of signal is seen in both potassium and nanoparticle channels when the nanoparticles are added, but there is no increased signal without the particles in control groups. Similar to these results, an increase in sodium concentration is seen at two hours and is coincident with an increase of intracellular fluorescence from the nanoparticles **Supporting Information Figure 2.12**.

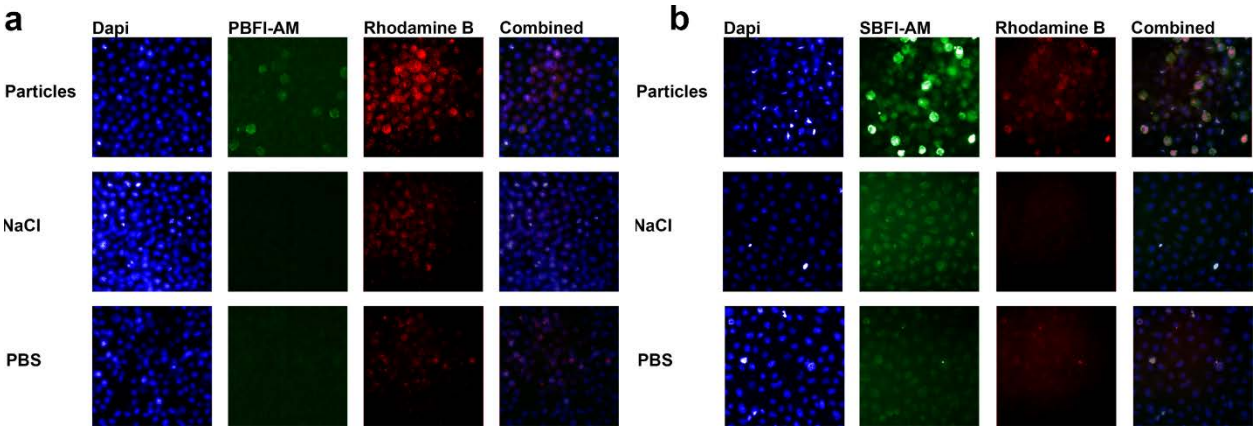

Figure 2.6 Nanoparticle uptake and ion increase Addition of nanoparticles significantly increases the concentration sodium and potassium in cells. This is correlated by tracking the intracellular increase of labeled nanoparticles

Determination of apoptotic or necrotic pathway of cellular death

Determination of cell death mechanism was carried out by staining with Annexin V-FITC (apoptosis), ethidium homodimer III(necrosis), and Hoechst 33342(nuclei). Increasing amounts of red, necrosis dye were seen at four and six hours **Figure 2.7a**. Significant levels of Annexin V-FITC binding were not seen as all time points displayed only background levels. Nuclei staining was apparent in all samples.

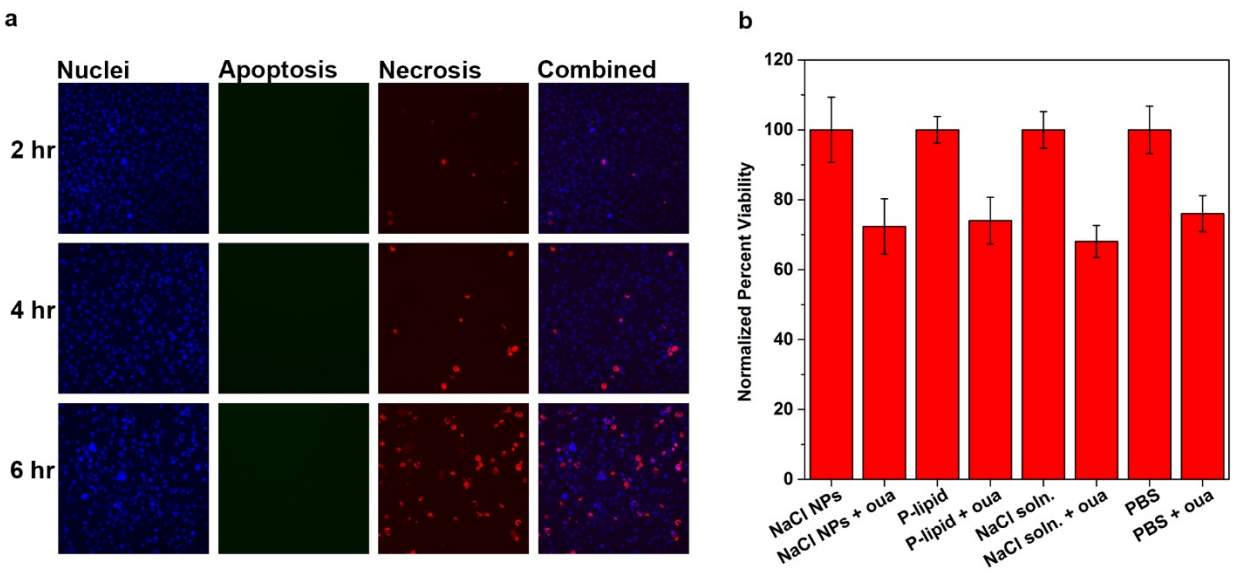

Figure 2.7 Apoptosis and Necrosis (a) Nuclei, apoptosis, and necrosis dyes. (b) Relative decrease in viability due to ouabain addition

Mitochondria health assessment

Mitochondria health was assessed by using MitoTracker® Green to image the distribution and number of mitochondria and JC-1 dye to determine the relative mitochondria membrane potential. 1 hour after particle addition the mitochondria are dispersed throughout the cells, but there is greater activity in samples with higher amounts of nanoparticles **Figure 2.8c**. By three hours significant signal has faded from the mitochondria in higher concentrations and the mitochondria appear to clustered close to the nucleus. After two hours at the highest concentration of NaCl NPs added significant loss of the red to green fluorescence ratio was observed **Figure 2.8a**. ATP quantification was carried out using a luminescence assay. Progressive loss of ATP concentration was found in cells exposed to increasing levels of NaCl NPs **Figure 2.8b**.

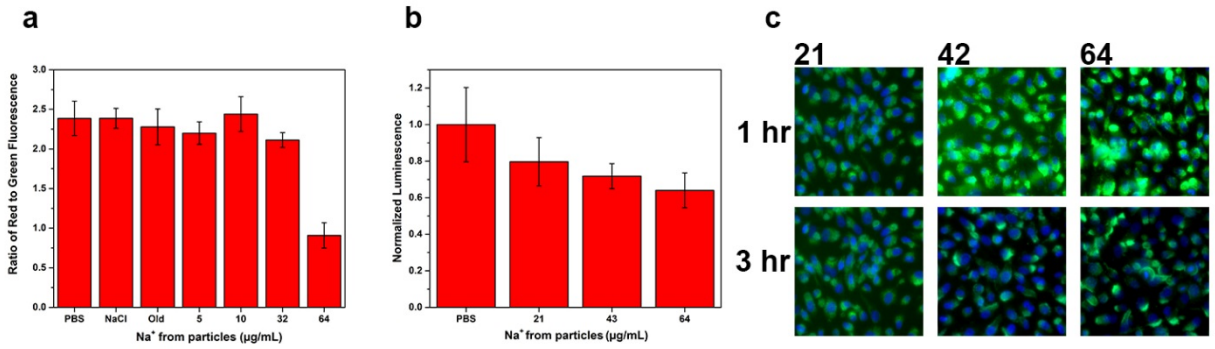

Figure 2.8 Mitochondrial health and ATP (a) JC-1 dye. (b) Relative ATP amounts. (c) Stained nuclei (blue) and mitochondria(green) at different times and different concentrations (µg/mL Na^+ added)

Na^+/K^+ ATPase pump activity on cell viability

A MTT assay was used to determine the changes in viability due to the addition of the Na^+/K^+ ATPase pump inhibitor ouabain. For all controls and active nanoparticles the decrease in viability with 10 nM ouabain added was ~30 percent **Figure 2.7b**.

Breast cancer animal model therapy

Tumor growth was consistent in PBS and aqueous NaCl controls and low concentrations of NaCl NPs. High concentrations of particles displayed a large decrease in tumor growth from six days after injection and maintained the lower size and growth rate throughout the experiment **Figure 2.9**. Animal weights remained similar throughout the experiment.

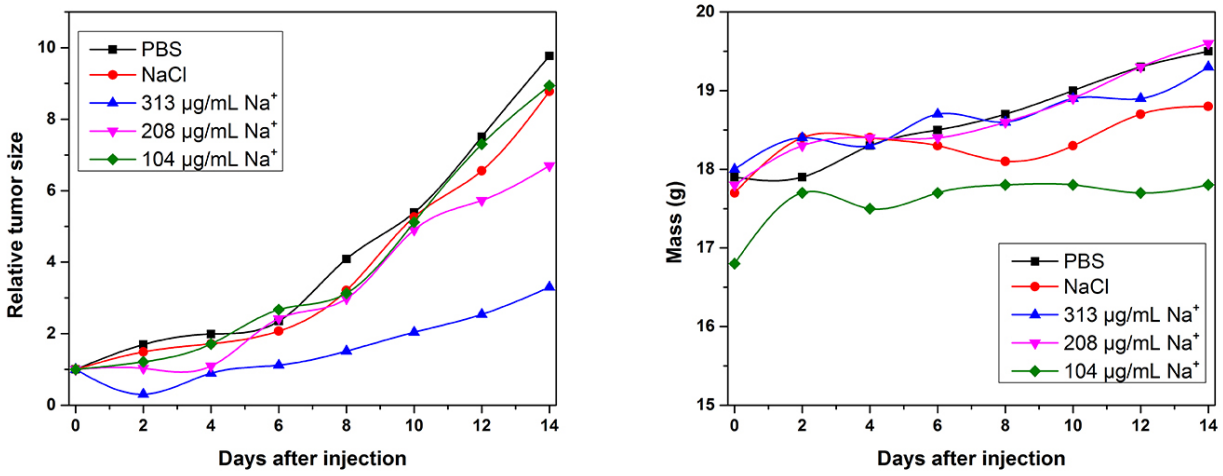

Figure 2.9 Tumor volume and animal weight (a) Relative volume of tumors compared to volume at day 0. (b) Mass of animals

Discussion

We report the first use of sodium chloride nanoparticles for biomedical applications. By using an aqueous-free environment in which to carry out the synthesis, the resulting particles are stable and well defined. Initial experiments using sodium oleate and thionyl chloride generated cubic nanoparticles. However, the low solubility of oleates in non-polar organic solvents limited purification efforts. We developed another NaCl NP synthesis in which 1,2-tetradecanediol is dissolved in hexanes and oleylamine. Molybdenum(V)chloride is added and the solution is stirred overnight. Particles are purified by centrifugation. TEM analysis shows the particles to be cubic with edge lengths of 50-100 nm. The particle composition was found to be sodium chloride by both XRD and SEM-EDS. As synthesized particles are only stable in non-polar organic solutions likely due to a layer of surface-adsorbed oleylamine. Oleylamine has seen

extensive use as a surface coordinating surfactant in the synthesis of magnetic and plasmonic nanoparticles[25].

Notably, the latter synthesis does not appear to contain a sodium source. ICP analysis of the individual reagents and solvent found sodium to be present in 1,2-tetradecanediol at 1%(m/m). The resulting amount of sodium delivered by the diol is therefore comparable to the amount delivered in the oleate synthesis. The alcohols from several diols could coordinate with the sodium allowing such a high level of impurity. We selected $MoCl_5$ due to the high amount of possible chloride delivery, the fact that molybdenum is an essential micronutrient, and solubility in the solvent system[26]. The release of sodium and evolution of chloride likely occurs in a concerted process. $MoCl_5$ exhibits a high affinity toward oxygen and is able to coordinate to one or more oxygen atoms in reactions or catalysis[27,28]. $MoCl_5$ reacts with alcohols forming trichloride dialkoxides[29]. Diols, such as 1,2-tetradecanediol, are likely to chelate to the molybdenum in a similar process. A possible structure of such a compound is shown in **Figure 2.10**.

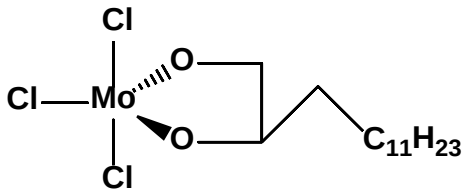

Figure 2.10 Suggested structure of molybdenum-diol complex

As the suggested sodium source is the coordinated binding of the diols, the introduction of $MoCl_5$ would weaken the sequestration of the cation allowing it to be released. Local evolution of chloride would enable rapid formation of NaCl sub-nano clusters in the non-polar solvent. Subsequent Ostwald ripening explains the increase in size from the sub-

nano to nanoscale. This form of growth has been theoretically modeled and witnessed in other nanoformulations[30,31].

To impart the particles with aqueous stability we used a PEGylated and amine terminated phospholipid. PEGylation both increases water stability and reduces uptake by the reticuloendothelial system[32]. Amine functionalization allows for rapid cell internalization and a possible site for conjugation of dye or targeting molecules[33].

It was found that coated nanoparticles display concentration dependent toxicity when added to PC3 prostate cancer cell lines. Notably, this toxicity relies on the length of time the particles have been suspended in aqueous solutions. Short incubation in PBS yields the highest reduction in viability while subsequently longer incubation times reduces toxicity to nearly baseline levels by eight hours. This data correlates well with TEM images of particles gradually dissolving after suspension in water and reinforces our hypothesis of NaCl nanoparticle toxicity. At early time points, particles appear similar to their as-synthesized predecessors. However, by two hours the morphology is significantly altered and salt deposits can be seen. Images from eight hours show very few intact particles, circular salt deposits are likely phospholipid micelles that have dried with salts inside them.

Live/dead assays demonstrate a rapid induction of toxicity between four and six hours after introduction of particles. According to our hypothesis, NaCl NPs should be internalized before this time point and release ions that ultimately lead to toxicity. Loading a sodium sensitive dye into cells enabled the visualization of intracellular sodium concentration increase in particle treated cells but not those treated with PBS or aqueous equal molar NaCl controls. Signal from rhodamine B labeled phospholipid

used to coat NaCl NPs were coincident with increase in sodium concentration, suggesting the increase is due to nanoparticle mediated delivery. Interestingly, at this same point intracellular potassium levels are increased. This likely stems from activation of Na^+/K^+ ATPase attempting to expel increased intracellular sodium. We used ouabain, a Na^+/K^+ ATPase inhibitor, to determine the toxicity differences in cell that were exposed to controls or NaCl NPs with or without the inhibitor. While there was a general decrease in viability with the addition of ouabain, the percent viability decrease for all controls and the active agent was nearly identical. This indicates the damage inflicted on the cells by the burst release of ions is too great for the pump to counteract.

One of the main targets of ionophore toxicity is the mitochondria. Dual labeling with mitochondria and nuclei dyes found that at early time points the mitochondria are dispersed throughout the cytoplasm with a roughly even distribution. At later points and with high NaCl NP concentrations mitochondria aggregated and the number was significantly reduced indicating damage. ATP synthesis and other mitochondria functions require a highly polarized mitochondrial membrane[34]. The dye JC-1 aggregates in the presence of polarized mitochondria to generate red fluorescence. In depolarized mitochondria JC-1 exists as a monomer with green fluorescence. Decrease in the ratio of red to green fluorescence is due to depolarization of the mitochondrial membrane is associated with apoptosis and necrosis[35]. After only two hours of incubation the red to green ratio in cells treated with high amounts of NaCl NPs decreased by more than 60%.

We next examined the cause of cell death. High activation of Na^+/K^+ ATPase coupled with compromised mitochondria health is expected to deplete the cell's ATP reserves thereby starving the cell for energy. We analyzed intracellular ATP concentations four hours after introduction of particles. A clear trend of increasing ATP depletion is visible from PBS controls to higher and higher amounts of added NaCl NPs. Apoptosis/necrosis assays showed membrane compromise indicative of necrosis, but little signal from apoptosis signaling from externalization of phosphatidylserine. As with live/dead assays, necrosis signal was minimal at early time points, but rapidly increased at six hours. A predominately necrotic pathway is normally not associated with ionophore mediated homeostasis disruption. Yet, there have been reports that inhibition of Na^+/K^+ ATPase may lead to cell death that has characteristics of both apoptosis and necrosis[12].

With these in vitro data suggesting a potential therapeutic for tumor therapy, we initiated a small proof-of-concept study to determine the possibility of in vivo use. To provide a more realistic test of the particle's ability we used a 4T1 breast cancer model in immunocompetent Balb/c mice. Mice were randomly selected for NaCl NP therapy or controls. Therapy mice were intratumorally injected with 50 µL NaCl NPs (313, 208, or 104 µg/mL Na^+ from NPs). Controls were injected with 50 µL PBS or 50 µL of aqueous NaCl (313 µg/mL Na^+ added). Controls and low concentrations of NaCl NPs displayed minimal deviations in tumor size. The highest concentration of NaCl NPs however, showed 2-3 fold reduction in tumor growth after two weeks. Throughout the treatment all animals were healthy with minimal differences in animal weight.

Conclusions

We reported the novel synthesis of sodium chloride nanoparticles for direct ion delivery to cancer cells. A unique aspect of this treatment is the rapid and total passivation of the active drug within 12 hours. After the particles have dissolved into constituent ions, there is no further toxicity. These nanoparticles are able to increase the concentration of intracellular sodium by bypassing the cellular membrane. After internalization, the particles break apart releasing high amounts of ions into the cytoplasm which disrupts ion homeostasis and damages mitochondria. The damaged mitochondria cannot generate sufficient ATP to fuel ion pumps and the cell eventually starves. We demonstrated that these particles maintain their effect in breast cancer animal models. Intratumoral injections of NaCl NPs was able to reduce the growth rate of tumors resulting in a 2-3 fold reduction in size after two weeks. These data suggest ion delivery mediated by nanoparticles as a new therapeutic modality for tumor management.

Supporting Information

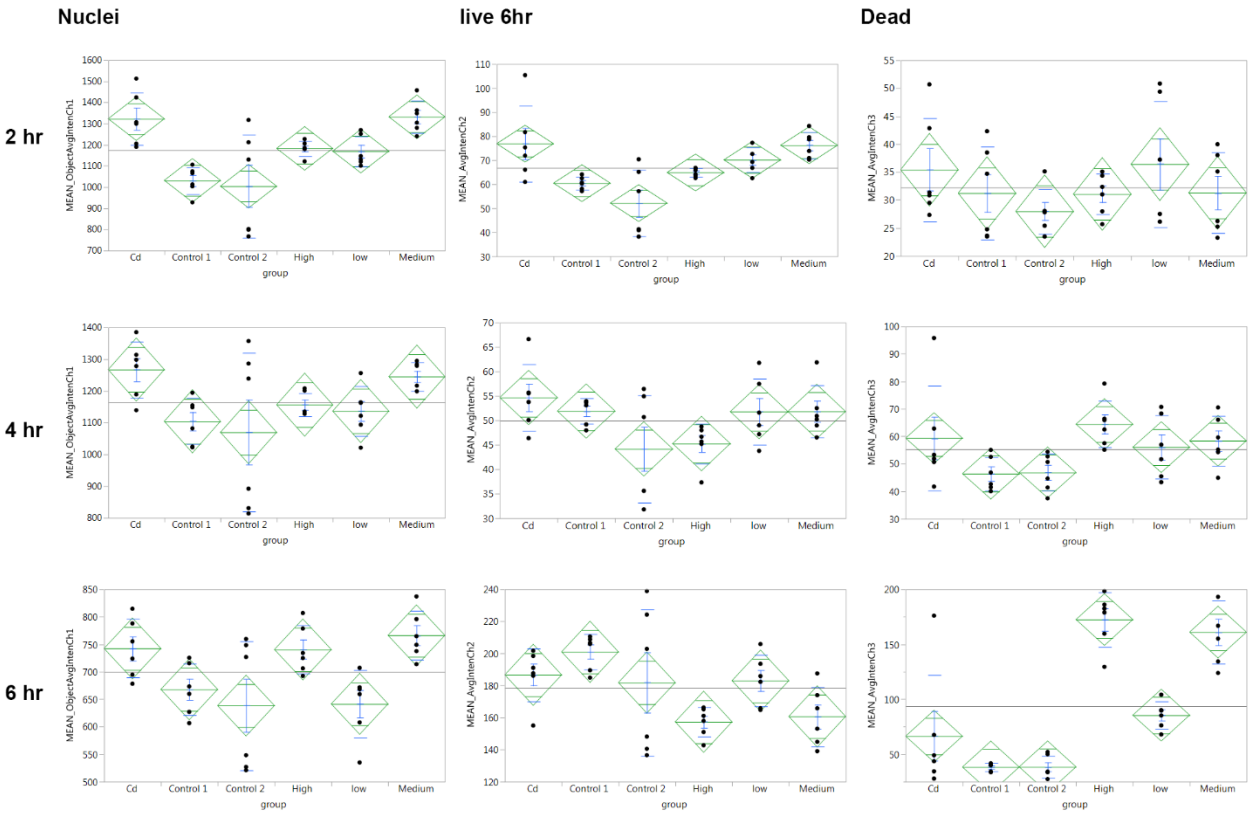

Figure 2.11 Quantification of nuclei, live, and dead dyes at 2,4, and 6 hours after particle addition

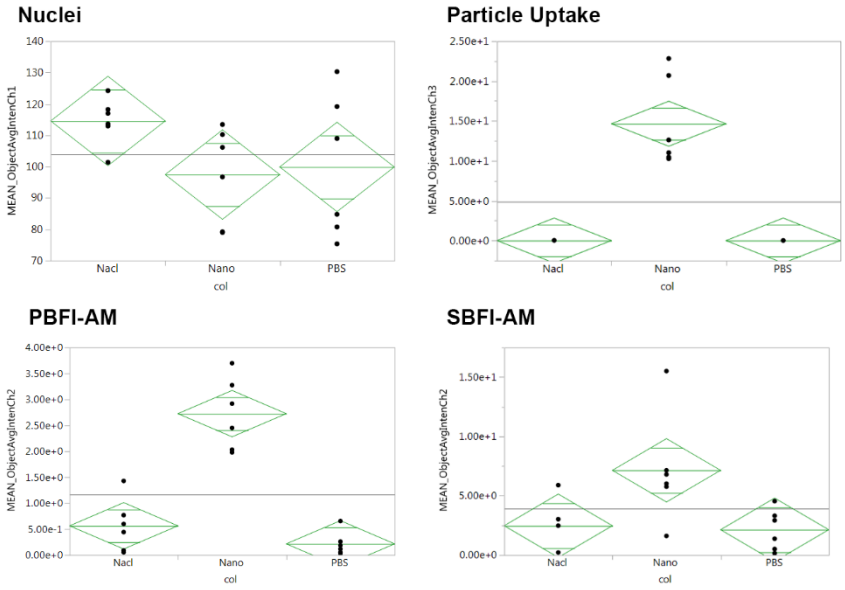

Figure 2.12 Quantification of dye intensities for nuclei, particle uptake, PBFI-AM, and SBFI-AM

References

(1) Milo, R.; Phillips, R.: *Cell biology by the numbers*.

(2) Vanwinkle, L. J.; Christensen, H. N.; Campione, A. L. *Journal of Biological Chemistry* **1985**, *260*, 2118-2123.

(3) Broer, S. *Physiol Rev* **2008**, *88*, 249-286.

(4) Demaurex, N. *News Physiol Sci* **2002**, *17*, 1-5.

(5) Pittman, J. K. *Front Plant Sci* **2012**, *3*.

(6) Lang, F.; Waldegger, S. *Am Sci* **1997**, *85*, 456-463.

(7) Strange, K. *Adv Physiol Educ* **2004**, *28*, 155-159.

(8) Catterall, W. A. *Neuron* **2000**, *26*, 13-25.

(9) Keating, M. T.; Sanguinetti, M. C. *Cell* **2001**, *104*, 569-580.

(10) Gouaux, E.; MacKinnon, R. *Science* **2005**, *310*, 1461-1465.

(11) Suhail, M. Na, *Journal of clinical medicine research* **2010**, *2*, 1-17.

(12) Chen, D. D.; Song, M. K.; Mohamad, O.; Yu, S. P. *Bmc Cancer* **2014**, *14*.

(13) Russell, J. B.; Houlihan, A. J. *Fems Microbiol Rev* **2003**, *27*, 65-74.

(14) Kart, A.; Bilgili, A. *J Anim Vet Adv* **2008**, *7*, 748-751.

(15) Strobel, H. J.; Russell, J. B. *Appl Environ Microb* **1989**, *55*, 2664-2668.

(16) Bergen, W. G.; Bates, D. B. *Journal of animal science* **1984**, *58*, 1465-1483.

(17) Smith, C. K.; Galloway, R. B. *J Parasitol* **1983**, *69*, 666-670.

(18) Mollenhauer, H. H.; Morre, D. J.; Rowe, L. D. *Biochimica et biophysica acta* **1990**, *1031*, 225-246.

(19) Iljin, K.; Ketola, K.; Vainio, P.; Halonen, P.; Kohonen, P.; Fey, V.; Grafstrom, R. C.; Perala, M.; Kallioniemi, O. *Clin Cancer Res* **2009**, *15*, 6070-6078.

(20) Gupta, P. B.; Onder, T. T.; Jiang, G. Z.; Tao, K.; Kuperwasser, C.; Weinberg, R. A.; Lander, E. S. *Cell* **2009**, *138*, 645-659.

(21) Fuchs, D.; Heinold, A.; Opelz, G.; Daniel, V.; Naujokat, C. *Biochemical and biophysical research communications* **2009**, *390*, 743-749.

(22) Griffin, T.; Raso, V. *Cancer Res* **1991**, *51*, 4316-4322.

(23) Griffin, T. W.; Richardson, C.; Houston, L. L.; Lepage, D.; Bogden, A.; Raso, V. *Cancer Res* **1987**, *47*, 4266-4270.

(24) Weingart, J.; Vabbilisetty, P.; Sun, X. L. *Adv Colloid Interfac* **2013**, *197*, 68-84.

(25) Mourdikoudis, S.; Liz-Marzan, L. M. *Chem Mater* **2013**, *25*, 1465-1476.

(26) Mendel, R. R. *Dalton T* **2005**, 3404-3409.

(27) Guo, Q. X.; Miyaji, T.; Hara, R.; Shen, B. J.; Takahashi, T. *Tetrahedron* **2002**, *58*, 7327-7334.

(28) Dolci, S.; Marchetti, F.; Pampaloni, G.; Zacchini, S. *Eur J Inorg Chem* **2013**, 1371-1380.

(29) Bradley, D. C.; Multani, R. K.; Wardlaw, W. *J Chem Soc* **1958**, 4647-4651.

(30) Dagtepe, P.; Chikan, V. *J Phys Chem C* **2010**, *114*, 16263-16269.

(31) Gentry, S. T.; Kendra, S. F.; Bezpalko, M. W. *J Phys Chem C* **2011**, *115*, 12736-12741.

(32) Jokerst, J. V.; Lobovkina, T.; Zare, R. N.; Gambhir, S. S. *Nanomedicine-Uk* **2011**, *6*, 715-728.

(33) Alexis, F.; Pridgen, E.; Molnar, L. K.; Farokhzad, O. C. *Mol Pharmaceut* **2008**, *5*, 505-515.

(34) Perry, S. W.; Norman, J. P.; Barbieri, J.; Brown, E. B.; Gelbard, H. A. *Biotechniques* **2011**, *50*, 98-+.

(35) Kroemer, G.; Galluzzi, L.; Brenner, C. *Physiol Rev* **2007**, *87*, 99-163.

CHAPTER 3

OSTEOARTHRITIS THERAPY USING CONTROLLED ION RELEASE FROM LITHIUM FLUORIDE NANOPARTICLES

Todd, T.; Chen, H.; Latremouille, J.; Zheng, L.; Xie, J. To be submitted to *Nature Chemistry*

Abstract

Despite being the smallest and lightest approved drug, lithium has an extensive history in medicine. Since the 1940s its salts have been used for the treatment of mania and depression. Yet concerns over the drug's toxicity due to lithium's small therapeutic window have prevented its translation to other diseases. Additionally, as an alkali metal, lithium is very difficult to deliver with a controlled, slow release profile due to its high solubility. We report the first disease site localized, controlled release of lithium for biomedical applications. We synthesized silica-coated lithium fluoride nanoparticles and injected the formulation into rat osteoarthritis joint models. This formulation was able to reduce damage from OA by down-regulating the production of catabolic proteinases. Our particles also displayed a more complete protection of the joint space compared to equal molar LiCl or clinically approved hyaluronic acid.

Introduction

Osteoarthritis(OA) currently affects more than 27 million people in the U.S. and is expected to increase in prevalence due to an aging population and increases in obesity[1,2]. Currently, this degenerative joint disease has no cure and ultimately results in significant loss of quality of life.[3,4] FDA approved medications, such as acetaminophen, Ibuprofen, celecoxib, and prednisone only treat the pain of the disease. While low grade osteoarthritis pain can be managed with NSAIDS or analgesics, the efficacy of these treatments is overwhelmed by the continually deteriorating joint space. Extended treatments can also lead to gastrointestinal issues and compromised renal ability[5-7]. The pain response in moderate stage OA is treated with intra-articular (IA) injections of

corticosteroids or hyaluronic acid (HA). Despite reports that HA can increase the synthesis of proteoglycans and inhibit phagocytosis by immune cells, HA is largely considered to reduce pain by down-regulating inflammatory mediators and replacing lost viscoelastic material[8]. When the course of treatment for these injected drugs is no longer sufficient, joint replacement surgery is the main remaining option. In 2009 alone, 905,000 knee and hip replacements were performed at a total cost of $42.3 billion[9]. Hence, there is an urgent need to develop a therapeutic that can impede the progression of the disease.

Recently, lithium has been indicated as a possible means of treating the damage associated with osteoarthritis[10-13]. Lithium has long been used in the clinic to treat bipolar disorder[14,15]. It was found that lithium reduces signaling of NF-κB and activation of p38 MAPK and STAT-3 which leads to lower expression of catabolic species that degrade cartilage[10,11]. The reduction of these catabolic species in IL-1β and TNF-α induced osteoarthritis models leads to protection of chondrocytes in vitro with a significant reduction in collagenolytic activity and collagen release. In vivo, lithium was found to minimize the loss of mechanical properties in excised rat joints and decrease the Osteoarthritis Research Society International (OARSI) histologic scores in the knee joints of mice[11,13]. Further work has suggested that lithium can inhibit Hedgehog signaling pathways by modulation of cilia on chondrocytes[12].

Despite the benefits of using lithium as a method of protecting chondrocytes from OA damage, administration of the drug is problematic. Systemic oral administration for bipolar affective disorder requires a narrow therapeutic serum lithium concentration to be maintained between 0.5 and 1.3 mM[16]. However, noticeable toxicity has been

shown in some patients with lithium concentrations within the normal therapeutic range and low grade lithium toxicity is considered to begin at serum concentrations of 1.5 mM[17,18]. In vitro studies have shown that 5 mM Li^+ is sufficient to significantly reduce collagenolytic activity, but 10 mM Li^+ is required for reduction of collagen release back to control levels[10]. Therefore administration by direct injection to the joint space, or intra-articular(IA) injection, was used to minimize side effects of systemic dosing while increasing the amount delivered to the joint. IA injection of lithium salts allows a higher therapeutic effect than oral administration in vivo as seen by a greater reduction in OARSI scores [11]. Though the increase in local concentration is beneficial, it has been found that the rate of distribution of small molecules to the circulation is similar to other injection methods[19,20]. Given the high mobility and small size of lithium it is expected to have a short retention time in the region. As the therapeutic effect of lithium is most notable at 10 mM, this relatively high concentration was injected weekly in previous animal experiments[11]. While the potential benefits of IA delivery of lithium are numerous, the high solubility of lithium makes therapy at safe concentrations difficult.

Herein, we report a novel approach for controlled release of Li^+ for effective and extended protection of chondrocytes. This is achieved using a silica coated LiF nanoparticles, or LiF@SiO_2. The unique nanostructure prevents fast liberation of Li^+ to the surroundings and instead allows for sustained release over a time period of 48 hours. The counter ion, fluoride, is efficiently sequestered by extracellular calcium, with minimal impact to local bones or distant organs. In a proof-of-concept study, we injected LiF@SiO_2 within HA gel to the joint of a rat OA model **Figure 3.1**. We observed minimal symptoms of joint degradation or damage in LiF treated animals. While controlled

release of small molecule drugs has been extensively investigated in nanomedicine, sustained release of ions and their impact in the therapy context has never been reported before. Our approach demonstrates the feasibility of nanoparticle mediated ion delivery, not only for arthritis management, but for all diseases that ion therapy could potentially be beneficial.

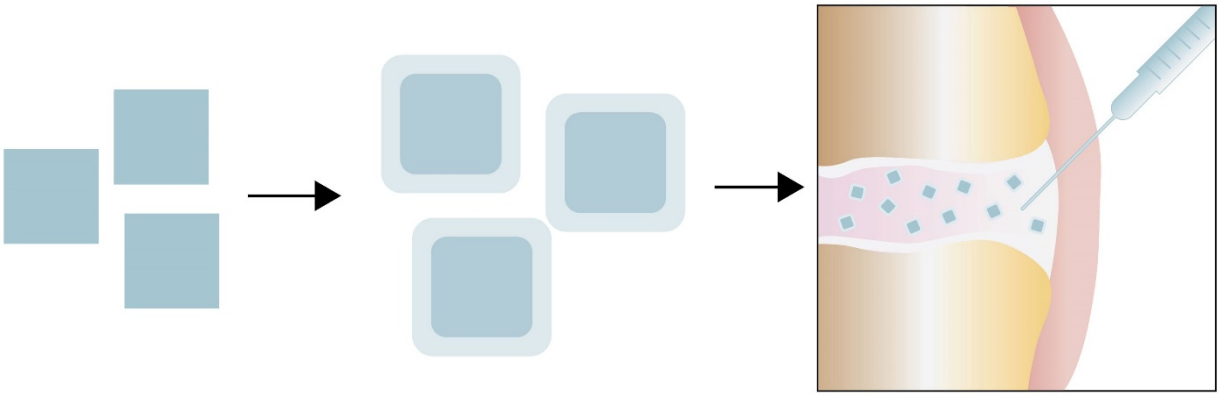

Figure 3.1 Schematic representation of LiF NP coating and subsequently injection into a diseased joint space.

Materials and methods

Lithium fluoride nanoparticle synthesis

The following procedure yields particles of ~150 nm. 1.0 mL of 0.250 M lithium nitrate in ethylene glycol was added to a plastic vial with 4 mL of ethylene glycol and 4 mL of poly(ethylene glycol) (average mw 300). A stir bar is added and the solution is mixed for 10 minutes. While stirring, 1.0 mL of 0.375 M ammonium fluoride in ethylene glycol is added. The vial is sealed and the stirring is continued for at least 1 hour. The particles are purified by centrifuging at 9000rpm (9682 rcf) for 10 minutes, decanting the supernatant, and then redispersing the particles in ethanol using brief sonication. This process is repeated 3x to ensure the removal of unwanted species. After the last

dispersal in 10mL ethanol, the particles are again sonicated and remain stable in solution at 4°C for at least one month.

Silica coating of LiF nanoparticles

As prepared nanoparticles in 10 mL of ethanol are sonicated for ~2 minutes to ensure full dispersion. 5 mL of the sonicated ethanolic LiF solution is added to a plastic vial with 5 µL of tetraethyl orthosilicate. The solution is sonicated for a further 2 minutes to ensure a homogeneous solution. A stir bar is added to the vial and the solution is rapidly stirred. 200 µL of 30% ammonium hydroxide solution is added dropwise and the resulting solution is allowed to mix overnight. The coated particles are purified by the same centrifugation procedure that is used for the LiF particles.

Lithium concentration analysis using ICP-MS

Lithium samples were dissolved in nitric acid (70%) for 24 hr and subsequently dried on a hotplate for another 24 hr. The dry remnants were dispersed in 5.00 mL of 5% nitric acid and tested by the Center for Applied Isotope Studies at UGA on a VG PlasmaQuad 3 ICP-MS.

Electron microscopy of LiF nanoparticles

LiF samples in ethanol were dried on formvar TEM grids at 50°C overnight for TEM and STEM imaging. TEM images were acquired on a FEI Tecnai 20 operated at 200kV at the Georgia Electron Microscopy center on the main campus of UGA. SEM images and elemental mapping were also taken at GEM on an FEI Teneo operating at 5

kV for images and 10 kV for elemental mapping. STEM data was collected on a Hitachi HD 2000 operating at 200kV.

Animals

Spraque Dawley Rats (SD rats) were obtained from Guangxi Medical University. All experiments were conducted in accordance with the guidelines of the Animal Committee and with ethics approval from the Guangxi Medical University Animal Care and Use Committee, China (Protocol Number: 2013-12-3). All of the procedures performed on these rabbits were approved by the Guangxi Medical University Animal Care and Use Committee.

Articular chondrocytes culture

Articular chondrocytes were isolated from joint of 1-week-old SD rats by enzymatic digestion. In brief, cartilage was trypsinized with 0.25% (v/v) trypsin (Solarbio) for 30 min and then dissociated with 2 mg/mL collagenase type II (Gibco) for 3h. After centrifugation, the chondrocytes were cultured in the media of alpha-modified Eagle's medium (α-MEM, Gibco) containing 20% (v/v) fetal bovine serum (FBS) (Gibco) and 1% (v/v) penicillin/streptomycin (Solarbio). The cells were transferred to the humidified incubator with 5% CO_2 at 37°C. The culture medium was replaced every other day. Articular chondrocytes at passage 2 were trypsinized and collected for further studies.

Cytotoxicity test

The 3-(4, 5)-dimethylthiahiazo (-z-y1)-3, 5-di-phenytetrazolium-romide (MTT, Gibco) method was used to study the cytotoxicity of LiF@$SiO_2$and LiF@SiO_2 in Hyaluronic Acid (HA)- on chondrocytes and determine the optimal concentration. Cells seeded in 96 well-plates were treated with LiF@SiO_2 at various concentrations (0.01-10 mM) with or without HA. Then, 20 μL of 5 mg/mL MTT reagent was added in 200 μL of test culture medium and incubated at 37°C for 4 h. 200 μL of DMSO was added to dissolve the formazan product after the supernatant was removed. The absorbance was measured on a microplate reader (Thermo Fisher Scientific) at 570 nm and the measurements were performed in sextuplicate. Optimal concentrations of LiF@SiO_2 were chosen for further study, which were 0.1mM, 1mM and 5mM.

IL-1β induced chondrocytes and treatment

The effects of LiF@SiO_2, LiCl and HA on IL-1β induction of chondrocytes were investigated in five groups of cells: (1) normal control：chondrocytes treated with medium only, (2) IL-1β: chondrocytes treated with 10 ng/mL IL-1β (Gibco, USA), (3) IL-1β+HA: chondrocytes pre-incubated with HA for 1 h followed by treatment with IL-1β for 2, 5, and 8 days, (4) IL-1β+LiCl : chondrocytes pre-incubated with 10 mM LiCl for 1 h followed by treatment with IL-1β for 2, 5, and 8 days, (5) IL-1β+LiCl/HA: chondrocytes pre-incubated with 10 mM LiCl and HA for 1 h followed by treatment with IL-1β for 2, 5, and 8 days, (6) IL-1β+LiF1: chondrocytes pre-incubated with 0.1mM LiF@SiO_2 for 1 h followed by treatment with IL-1β for 2, 5, and 8 days , (7) IL-1β+LiF2: chondrocytes pre-incubated with 1mM LiF@SiO_2 for 1 h followed by treatment with IL-1β for 2, 5, and 8 days, (8) IL-1β+ LiF3 : chondrocytes pre-incubated with 5 mM LiF@SiO_2 for 1 h

followed by treatment with IL-1β for 2, 5, and 8 days, (9) IL-1β+LiF/ HA1 : chondrocytes pre-incubated with 0.1 mM LiF and HA for 1h followed by treatment with IL-1β for 2, 5, and 8 days, (10) IL-1β+LiF/HA2: chondrocytes pre-incubated with 1 mM LiF and HA for 1h followed by treatment with IL-1β for 2, 5, and 8 days,(11) IL-1β+LiF/HA3: chondrocytes pre-incubated with 5 mM LiF and HA for 1h followed by treatment with IL-1β for 2, 5, and 8 days,.

OA induction and animal treatment

Two hundred and forty eight male SD rat weighing 180 ± 20 g were used in this study. After anesthetized, two hundred and forty randomly selected rats were underwent bilateral anterior cruciate ligament transection (ACLT) on the knee joints to induce OA and were randomly assigned to ten groups. The other eight were underwent sham operations (normal group), in which the articular cavity was opened and sutured with the short anterior cruciate ligament intact. At 4, 8 and 12 weeks after surgery, the animals were received intra-articular injections of 50 μL 1)10mg/mL HA (HA group), 2) 10mM LiCl (Cl group), 3)10mM LiCl +HA (ClH group), 4) 0.1mM LiF@SiO_2 (LiF1 group), 5)1mM LiF@SiO_2 (LiF2 group), 6)5mM LiF@SiO_2 (LiF3 group), 7)0.1mM LiF@SiO_2 +HA (LiF/HA1 group), 8)1mM LiF@SiO_2 +HA (LiF/HA2 group) or 9)5mM LiF@SiO_2 +HA (LiF/HA3 group) (the dose identified as exhibiting the best performance in the in vitro study) in both knees once per week for 4, 8 and 12 weeks. The OA Model group was injected with 50 μL of PBS alone under the same conditions. In the normal group, no other procedures were conducted. The animals in the eleven groups were sacrificed at 4, 8 and 12 weeks after therapy.

Quantitative real-time PCR (qRT-PCR) detection

Genetic information was analyzed by real-time quantitative reverse polymerase chain reaction (qRT-PCR). Primer sequences and number are presented in **Table 1**. After 2, 5 and 8 days of treatment, cells were washed once with PBS. An RNA isolation kit (Tiangen Biotechnology) was used for total RNA extraction. About 300 ng total RNA was used as template with a reverse transcription kit (Fermentas) for reverse transcription. The qRT-PCR reactions were carried out using a Quantitative PCR Detection System (Realplex 4, Eppendorf Corporation) with FastStart Universal SYBR Green Master (Mix, Roche company) at condition of 10 min at 95°C, 15 s at 95°C and 1 min at 60°C. Simultaneously, data of melting curve were collected for PCR specificity verification. Each experiment was repeated in triplicate to reduce operation bar errors. The 2-ΔΔCT method was used to calculate qRT-PCR validation. The gene expression were normalized based on the cycle threshold (CT) values for each gene and glyceraldehyde-3-phosphate dehydrogenase (GAPDH).

Results

Lithium fluoride nanoparticle synthesis, coating, and characterization

Lithium fluoride particles were synthesized by a precipitation reaction in an ethylene glycol (EG)/poly ethylene glycol (PEG) solution. Altering the ratio of EG to PEG allows for control over particle size, with higher ratios yielding larger particles and lower ratios yielding smaller ones **Figure 3.2a-c**. The particles can be coated with a ~20 nm layer of silica **Figure 3.2d**. Coated particles were used in all subsequent experiments. Particle composition was determined by X-Ray diffraction both before and

after silica coating **Figure 3.2e**. High resolution SEM shows homogeneous cube-like structures **Figure 3.2f**. Low resolution SEM and elemental mapping of fluorine and oxygen further comfirm the particle composition and suggest a PEG coating. **Figure 3.2g-i**

Lithium fluoride nanoparticle degradation and fluoride sequestration

STEM imaging with EDS analysis was used to determine changes to the composition of LiF nanoparticles when exposed to representative amounts of extracellular calcium. It was found that calcium quickly formed nanoparticles with fluoride yielding calcium fluoride **Figure 3.3a-f**. ICP-MS results demonstrated that LiF particles rapidly dissolve in aqueous solutions, but LiF@SiO_2 particles display a half-life of ~24 hours even when exposed to calcium and hyaluronic acid **Figure 3.3g**.

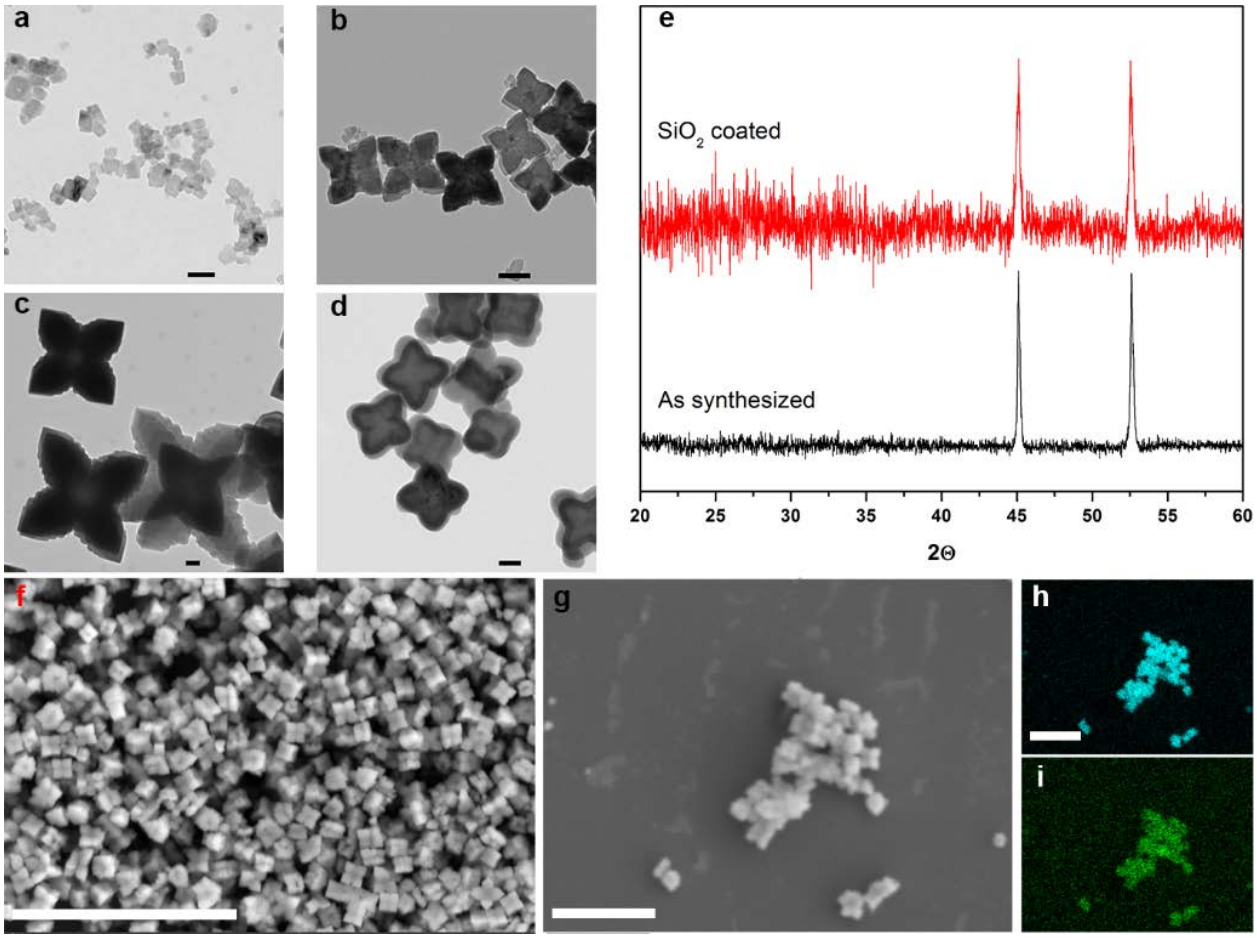

Figure 3.2 Characterization of LiF NPs Size of LiF NPs can be altered from 50 nm to >1 µm (a-c). As synthesized LiF NPs can be coated with a layer of silca(d). TEM scale bars: 100 nm. XRD of as synthesized and silica coated LiF NPs(e). High(f) and low(g) resolution SEM. Elemental mapping for fluoride(h) and oxygen(i). SEM scale bars: 2.5 µm.

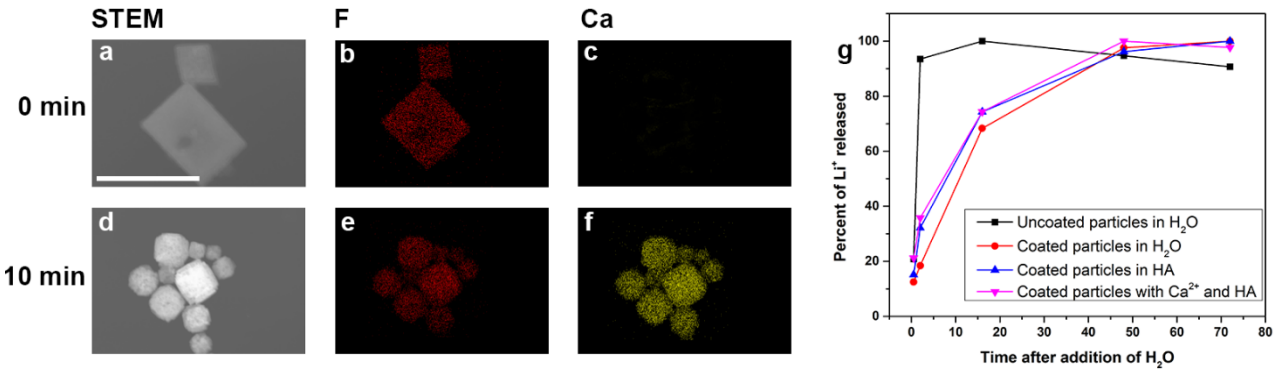

Figure 3.3 STEM elemental mapping and Li^+ release STEM and elemental mapping show rapid increase of Ca^{2+} when exposed to 1.5 mM $Ca(NO_3)_2$. Lithium is rapidly released from uncoated LiF, but slowly from $LiF@SiO_2$.

Effect of LiF and LiF + HA on cell viability

Evaluation of chondrocytes' viability using MTT assay was performed to determine acceptable concentrations of $LiF@SiO_2$ for further use **Figure 3.4**. The nanoparticles displayed negligible toxicity compared with the control group up to 10 mM. When combined with HA the viability of the cells dropped to 60% at 10 mM. Based on these results we selected LiF dosages of 0.1, 1.0, and 10 mM LiF for further evaluation.

Expression levels of OA markers in samples treated by $LiF@SiO_2$

The gene expression levels of MMP-3, MMP-13, and TIMP-1 in response to incubation with 10 mM LiCl and 0.1 mM LiF in OA models were determined by qRT-PCR. (**Table 3.1** gives the primer sequences used) **Figure 3.5f** displays the increase in gene expression of MMP-3 and MMP-13 and the decrease of TIMP-1 in trials with no lithium

addition. Aqueous LiCl shows elevated levels of MMP-3 and MMP-13, but the values are reduced compared to IL-1β controls. LiCl and LiF both increase the expression of TIMP-1, but in LiF the increase is nearly 175% of the baseline compared to 125% for LiCL samples. Levels of MMP-3 and MMP-13 are nearly at baseline in LiF treated cells.

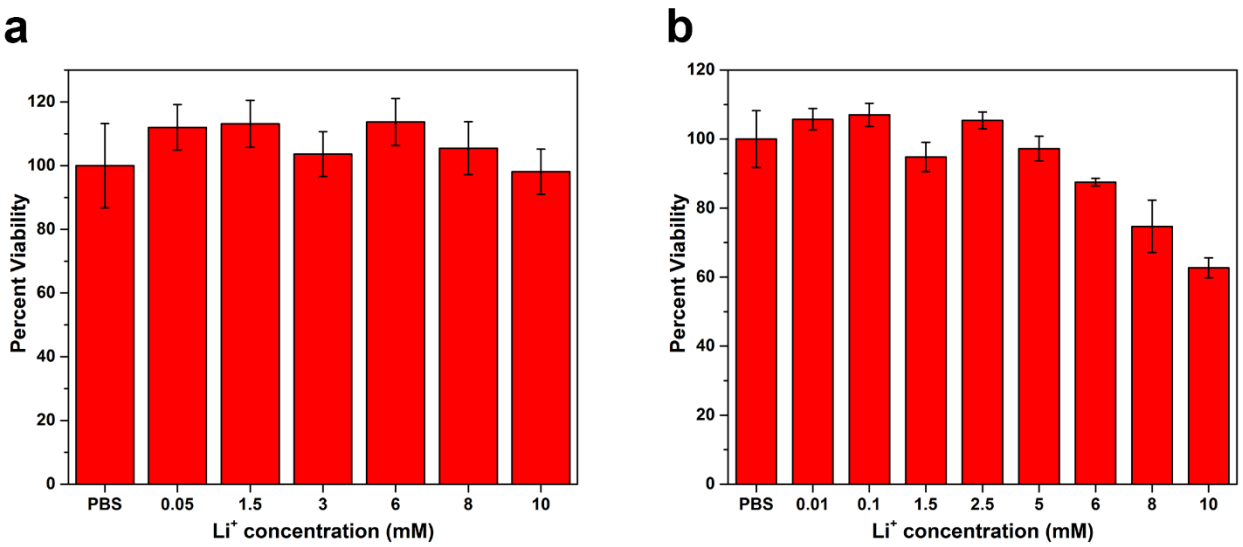

Figure 3.4 MTT viability assay MTT assay shows minimal toxicity to chondrocytes of SiO_2@LiF at relevant doses(a). Viability decreases with the addition of HA(b).

Table 3.1 Primers for qRT-PCR

Gene name	Forward primer	Reverse primer
MMP-1	5'-GGACTTGCTCACACATTCCCA -3'	5'- GAGTGAGTCCAAGGGAGTGG -3'
MMP-3	5'- GGCTGTGTGCTCATCCTACC -3'	5'- TGGAAAGGTACTGAAGCCACC -3'
MMP-13	5'- GGATCCATGATGGCACTGCT -3'	5'- TGGCTTTTGCCAGTGTAGGT -3'
TIMP-1	5'- GCTTTCTGCAACTCGGACCT-3'	5'- TCTCCATGGCTGGGGTGTAG -3'

MMP-1 expression in response to IL-1β exposure in chondrocytes

Immunohistochemical analysis was used to show the up or down regulation of MMP-1 in chondrocytes that have been exposed to IL-1β **Figure 3.5a-e**. In the cells

that were only exposed to IL-1β significantly higher staining (dark brown color) is visible in comparison to the control. This result and the lower staining of MMP-1 in LiCl and LiF treated cells correlates well with the qRT-PCR data. Notably, the difference in MMP-1 expression between cells treated with only IL-1β and cells treated with both HA and IL-1β is minimal.

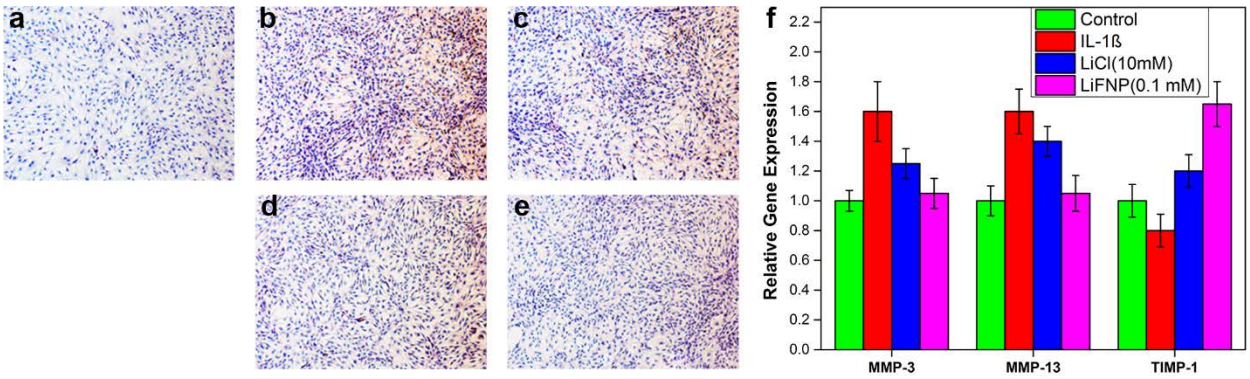

Figure 3.5 MMP expression Immunohistochemical staining for MMP-1(a-e): (a) control, (b) IL-1β, (c) hyaluronic acid, (d) 10 mM LiCl + HA, (e) 10 mM LiF + HA. qRT-PCR of MMP-3, MMP-13, and TIMP-1(f).

Macroscopic observation of articular cartilage in response to LiF

Animal models with OA induced by ACLT surgery were used to determine the effect of LiF@SiO_2 particles on the progressive joint degradation associated with the disease **Figure 3.6**. Animals with no treatment showed minimal pathology one month after the surgery but significant joint destruction, erosion, and osteophyte formation at three months. HA treated animals displayed less damage at three months but several osteophytes were visible. In both the LiCl + HA and LiF + HA injected animals there was minimal damage at three months.

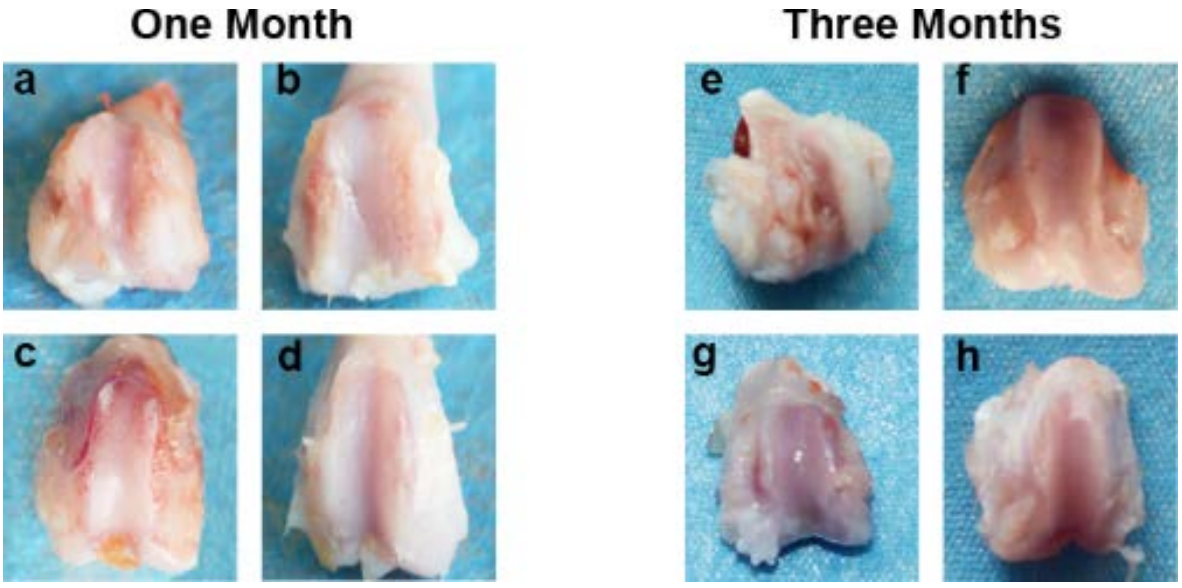

Figure 3.6 Excised joints from animals All joints appear healthy one month after surgery. At three months the control joint has noticeable erosion, destruction, and osteophyte formation. Hyaluronic acid displays significantly less damage, but a several osteophytes are visible. Both lithium treated joints have minimal apparent damage. One month joints are labeled as follows: (a) Control, (b) HA, (c) 10 mM LiCl + HA, (d) 1 mM LiF + HA. Three month joints are labeled: (e) control, (f) HA, (g) 10 mM LiCl + HA, (h) 1 mM LiF+ HA.

Discussion

There is a critical, unmet need for drugs that can reduce the joint damage associated with OA. Reports have shown in vitro and in vivo that lithium has powerful chondro-protective effects by down-regulating numerous chemokines and cytokines that are implicated in the progression of OA. Given the short residence time of aqueous lithium in the joint space, we synthesized nanoparticles with high lithium loading and delayed release. A simple precipitation reaction between solutions of lithium nitrate and

ammonium fluoride in ethylene glycol provided large, 1 micron particles **Figure 3.1c**. We discovered that addition of low molecular weight poly(ethylene glycol) (PEG, MW 300) yielded smaller, monodisperse nanoparticles, down to 50 nm **Figure 3.1a,b**. XRD analysis confirmed that LiF is the composition of the particles **Figure 3.1e**. Despite the relatively low solubility of LiF compared to the other lithium halogen salts, it was found that lithium was released rapidly in dialysis testing **Figure 3.2g**. To impede this rapid breakdown we coated the LiF particles with a layer of silica **Figure3.1d**. The particle composition was not changed by the coating process as seen by XRD **Figure 3.1e**. Notably, the coating is amorphous silica which is not seen in the XRD spectra. These coated particles were able to greatly retard the release of Li^+ from 1 hr to 48 hr even in the presence of Ca^{2+} **Figure 3.2g**. Release of fluoride in the joint space was a potential concern in the selection of LiF particles. However, it was found that extracellular calcium concentrations (1.5 mM) were able to sequester the released fluoride **Figure 3.2a-f**. The high loading of lithium, controlled and extended release, and tunable size suggests the possible use of these particles as a delivery vehicle for Li^+ based OA therapy.

This study demonstrates the ability of lithium fluoride nanoparticles to maintain the efficacy of free Li^+ in vitro in IL-1β induced cartilage damage. MTT viability assays verify that the introduction of LiF@SiO_2 NPs induces minimal toxicity to chondrocytes **Figure 3.3**. In agreement with previous publications, dissolved LiCl was found to inhibit the expression of MMP-1, MMP-3, and MMP-13 and increase the amount of TIMP-1 produced **Figure 3.4**[10,11]. These MMP's are implicated in the damage of cartilage whereas TIMP-1 reduces the expression of the chondro-destructive MMPs[21].

LiF@SiO_2 nanoparticles exhibited an even greater inhibition of MMPs and a higher expression of TIMP-1 than LiCl. The high efficacy of Li^+ delivery and minimal toxicity suggested the continuation of studies into OA animal models.

ACLT models of OA were used to determine the effect of LiF@SiO_2 on cartilage degradation and joint damage. While therapeutics that reduce damage to the joint are highly desired, they do not provide significant reduction in pain for the patient[22,23]. Therefore, the subsequent experiments were performed in HA solutions. Minimal differences between controls and treatment groups were visible on excised joints one month after ACLT surgery **Figure 3.5**. However, three months after the operation, the joint space on un-treated animals was noticeably damaged with significant roughness of the joint and osteophyte formation. HA treated animals showed less roughness in the joint space, but several osteophytes were apparent **Figure 3.5f**. LiCl and LiF@SiO_2 both co-injected with HA resulted in minimal damage to the joint space. Notably, the concentration of injected lithium required to protect the joints from visible damage was an order of magnitude lower when using LiF@SiO_2 compared to LiCl.

Conclusion

We have demonstrated the first use of nanoparticles explicitly for delivery of lithium for a biomedical application. The nanoparticles' size is readily controllable through introduction of poly (ethylene glycol) and with silica coating can gradually release the lithium payload over 48 hr. In vitro the particles are non-toxic at therapeutic concentrations and are able to minimize the release of cartilage-degrading MMPs. In vivo, the particles prevent significant damage to the joint space and do so 10x more

effectively than an equal molar injection of LiCl. Our preliminary investigation suggests the benefits of using LiF@SiO_2 NPs as a therapeutic against OA, however further studies need to be performed exploring the long-term effects of this therapy.

References

(1) Lawrence, R. C.; Felson, D. T.; Helmick, C. G.; Arnold, L. M.; Choi, H.; Deyo, R. A.; Gabriel, S.; Hirsch, R.; Hochberg, M. C.; Hunder, G. G.; Jordan, J. M.; Katz, J. N.; Kremers, H. M.; Wolfe, F.; Workgrp, N. A. D. *Arthritis Rheum* **2008**, *58*, 26-35.

(2) Hunter, D. J.; Neogi, T.; Hochberg, M. C. *Arthrit Care Res* **2011**, *63*, 31-38.

(3) Seed, S. M.; Dunican, K. C.; Lynch, A. M. *Formulary* **2009**, *44*, 143-+.

(4) Luyten, F. P.; Tylzanowski, P.; Lories, R. J. *Bone* **2009**, *44*, 522-527.

(5) Bradley, J. D.; Brandt, K. D.; Katz, B. P.; Kalasinski, L. A.; Ryan, S. I. *New Engl J Med* **1991**, *325*, 87-91.

(6) Fries, J. F. *New Engl J Med* **1999**, *341*, 1397-1398.

(7) Perneger, T. V.; Whelton, P. K.; Klag, M. J. *New Engl J Med* **1994**, *331*, 1675-1679.

(8) Moreland, L. W. *Arthritis Res Ther* **2003**, *5*, 54-67.

(9) Murphy, L.; Helmick, C. G. *Am J Nurs* **2012**, *112*, S13-S19.

(10) Hui, W.; Litherland, G. J.; Jefferson, M.; Barter, M. J.; Elias, M. S.; Cawston, T. E.; Rowan, A. D.; Young, D. A. *Rheumatology* **2010**, *49*, 2043-2053.

(11) Minashima, T.; Zhang, Y.; Lee, Y.; Kirsch, T. *Arthritis Rheumatol* **2014**, *66*, 1228-1236.

(12) Thompson, C. L.; Wiles, A.; Poole, C. A.; Knight, M. M. *Faseb J* **2016**, *30*, 716-726.

(13) Thompson, C. L.; Yasmin, H.; Varone, A.; Wiles, A.; Poole, C. A.; Knight, M. M. *J Orthop Res* **2015**, *33*, 1552-1559.

(14) Geddes. (vol 161, pg 217, 2004). *Am J Psychiat* **2004**, *161*, 1517-1517.

(15) Marmol, F. *Prog Neuro-Psychoph* **2008**, *32*, 1761-1771.

(16) Oruch, R.; Elderbi, M. A.; Khattab, H. A.; Pryme, I. F.; Lund, A. *European journal of pharmacology* **2014**, *740*, 464-473.

(17) Finley, P. R.; Warner, M. D.; Peabody, C. A. *Clin Pharmacokinet* **1995**, *29*, 172-191.

(18) Timmer, R. T.; Sands, J. M. *J Am Soc Nephrol* **1999**, *10*, 666-674.

(19) Schurman, D. J.; Kajiyama, G. *J Orthop Res* **1985**, *3*, 185-188.

(20) Coleman, P. J.; Scott, D.; Ray, J.; Mason, R. M.; Levick, J. R. *J Physiol-London* **1997**, *503*, 645-656.

(21) Aigner, T.; Zien, Z.; Gehrsitz, A.; Gebhard, P. M.; McKenna, L. *Arthritis Rheum* **2001**, *44*, 2777-2789.

(22) Goldring, M. B.; Berenbaum, F. *Curr Opin Pharmacol* **2015**, *22*, 51-63.

(23) Matthews, G. L.; Hunter, D. J. *Expert Opin Emerg Dr* **2011**, *16*, 479-491.

CHAPTER 4

IRON OXIDE NANOPARTICLE ENCAPSULATED DIATOMS FOR MAGNETIC DELIVERY OF SMALL MOLECULES TO TUMORS

[1] Todd, T.; Zhen, Z.; Tang, W.; Chen, H.; Wang, G.; Chuang, Y-J.; Deaton, K.; Pan, Z.; Xie, J. *Nanoscale*, 2014, **6**, 2073-2076 – Reproduced by permission of The Royal Society of Chemistry, DOI: 10.1039/C3NR05623F

Abstract

Magnetic targeting of therapeutics has been proposed as a non-invasive method of accumulating large amounts of drug into disease sites. The synthesis of metal and metal-oxide nanoparticles with high magnetic moment has provided a means with which to translate the theory to practice. Yet, using these nanoparticles for in vivo targeting has yielded disappointing results. Even loading iron-oxide particles onto larger silica carriers proves to be minimally effective. We show that diatoms, the silica skeleton of algae, can load enough iron oxide nanoparticles to make magnetic targeting a reality. Small molecules can be co-loaded with iron oxide nanoparticles onto diatoms. With an external magnetic field, the diatoms, after systemic administration, can be attracted to tumors. This study suggests a great potential of diatoms as a novel and powerful therapeutic vehicle.

Despite intensive research endeavors, cancer remains one of the leading causes of death in the United States.[1] One primary challenge in cancer therapy is to deliver therapeutics to tumors site-specifically without affecting normal tissues. The advantages offered by nanotechnology provide a great opportunity for addressing the current limitations of chemotherapy. With nanoparticles as carriers, drugs can stay in the circulation for extended periods of time and preferentially egress into tissues at tumor sites where blood vessels are more permeable.[2] This, in conjugation with malfunctioning lymphatic drainage, leads to preferable drug accumulation in tumors, the so-called enhanced permeability and retention (EPR) effect, which has been the dominant tumor targeting mechanism used by contemporary nanotherapeutics.[3, 4] Over the past decade, many types of nanoparticles have been investigated as drug vehicles.

Among them, porous silica nanoparticles have attracted much attention for their low toxicity, biodegradability, and easy fabrication.[5–7] With advanced technologies, silica nanoparticles can be prepared with different dimensions, geometries, and controllable pores on the surface for efficient drug loading.[8]

The efficiency of EPR-mediated tumor accumulation is heavily dependent on tumor vasculature permeability.[9, 10] This characteristic, however, varies drastically among tumor origins, stages, organs, and even across the same masses. Underestimation of this heterogeneity often results in failed translation and lower-than-expectation treatment efficacy with nano-therapeutics.[9] There have been efforts to develop “smart” nano-carriers by conjugating a tumor targeting motif onto particles surfaces’. This active targeting approach, though it may improve tumor cell selectivity, does not necessarily increase nanoparticles’ tumor accumulation.[11] Hence, there is an urgent need to develop a means to improve the delivery efficacy.

One promising approach in this context is magnetic delivery. The concept is to tag drug carriers with magnetic nanoparticles, after which the drugs can be summoned preferably to tumors by applying an external magnetic field at the sites. Magnetic modulation of particle movement has proven to be feasible with iron oxide nanoparticle (IONP)-loaded silica nanoparticles in vitro.[12, 13] Using this method for in vivo delivery, however, has met challenges. Commonly used silica nanoparticles have a size around 50–100 nm, and can load very limited numbers of IONPs. Such light loading leads to weak magnetic attraction, making magnetotaxis insufficient for in vivo delivery, given a complicated biological environment.

Here we tackle this issue by using diatoms as novel silica vehicles. Diatoms are a major group of algae that are encased within a silica shell called a frustule. Intact diatom shells have a length of approximately 10 μm with ~500 nm pores orderly populating their structure. With their much larger size, diatoms, as a carrier, can load significantly higher payloads than common silica nanoparticles. This includes encapsulating hundreds of magnetic nanoparticles per diatom,[14] and in doing so, granting the diatom with a superior magnetic response. In this proof-of-concept study, we successfully loaded a large amount of dye molecules as drug mimics onto IONP-tagged diatoms. Using fluorescence imaging and magnetic resonance imaging (MRI), we confirmed, in small animal tumor models, that these diatoms can be attracted to tumors by magnetic guidance **Scheme 4.1**

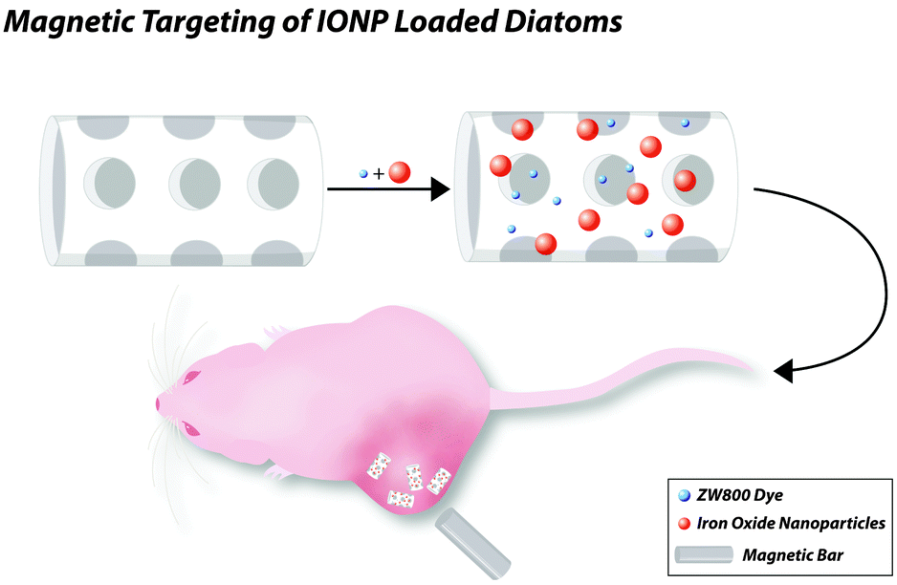

Figure 4.1 Schematic representation of IONP loaded diatoms for magnetic drug delivery. IONPs and small molecule drugs can be loaded into diatom frustules. In response to an external magnet, these diatoms are attracted to tumors after tail vein injection.

For preparation, raw diatoms (100% Food Grade) were first sonicated and repeatedly washed. Filter paper with 8 μm pores was then used to remove small and broken diatoms. **Figure 4.2 (a,b)** are scanning electron microscope (SEM) images of the purified diatom particles. The frustule shell has a thickness of 2 μm, which wraps to form a hollow cylinder, with an opening at one end. Lengths of the diatoms range from 5 to 15 μm. ~500 nm pores are orderly distributed across the particle's surface, both on the walls and on the edges.

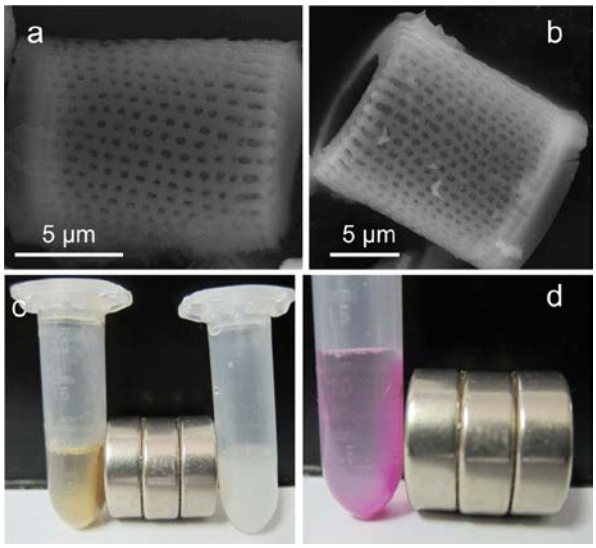

Figure 4.2 (a) & (b) SEM images of diatom particles. (c) Photograph of effect of magnetic field on IONP-DTMs (left) and unloaded diatoms (right). Without the addition of IONPs, no attraction to the magnet occurs. (d) Rhodamine B can be efficiently onto IONP-DTMs. With the use of a magnet, rhodamine B was attracted to the wall along with the IONP-DTMs.

.

For magnetic labeling, ~15 nm human serum albumin (HSA) coated IONPs were used. The synthesis and surface modification of the IONPs were reported by us previously.[15] Briefly, IONPs were made by thermal decomposition and were coated with a layer of oleic acid/oleylamine. These nanoparticles were surface-exchanged with dopamine in a 2:1 $CHCl_3$/DMSO mixture. The resulting, dopamine coated IONPs were dropwisely added to an aqueous solution of HSA, where the proteins were adsorbed onto the particle surface to grant them with good aqueous stability.

These HSA-IONPs were incubated with diatoms in PBS at room temperature for 2 h. As shown in our previous studies, due to multiple amine groups on the surface, HSA-IONPs are partially positively charged, and may interact with negatively charged surfaces (e.g. cell membranes[15]). It is expected that a similar electrostatic interaction can facilitate the binding of IONPs to the external and internal surfaces of diatom particles. At the end of the incubation, the solution was subjected to centrifugation at a moderate speed to enrich diatoms but not free IONPs. The products, IONP-loaded diatoms (IONP-DTMs), were washed by PBS to remove loosely bound IONPs.

IONP-DTMs were visualized by SEM. Many small particles were found on the diatom surface, which are attributed to immobilized IONPs (**Figure 4.6a**). The successful loading was also confirmed by energy-dispersive X-ray (EDX) spectroscopy (**Figure 4.6b**), and more convincingly, by inductively coupled plasma (ICP) analysis, revealing a Fe loading rate of ~8 wt%. Such heavy loading of IONPs made diatoms very sensitive to magnetic summoning. **Figure 4.2c** shows that when a magnetic bar was applied, IONP-DTMs were immediately attracted to the wall of the vessel. By contrast, individually dispersed HSA-IONPs were much less responsive to the magnetic attraction

(**Figure 4.7**). Due to a high loading capacity, the loading of IONPs does not affect the ability of diatoms to load small molecules. **Figure 4.2d** shows a study where rhodamine B, a red small molecule dye used as a drug mimic, was co-loaded with HSA-IONPs onto diatoms. The dye, as a payload, was magnetically attracted to the wall using a magnetic bar.

Next, we studied the cytotoxicity of IONP-DTMs with 4T1 murine breast cancer cells by 3-(4,5-dimethylthiazol-2-yl)-2,5-diphenyltetrazolium bromide, or MTT assays. Within the tested concentration range (0–625 μg/mL, based on the total mass), the cells kept over 80% viability after 24-h an incubation (**Figure 4.3**). This good biocompatibility is not unexpected given that both silica and HSA-IONPs were low-toxic.[16, 17]We also studied the biodegradability of diatoms in a body fluid mimic.[18] After one-week incubation, we found many broken nanostructures, indicating an ongoing degrading process (**Figure 4.8**). Given their relatively large size, however, complete degradation takes a longer time.

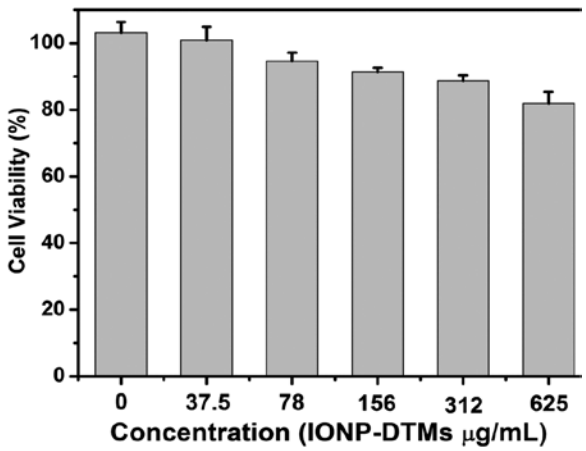

Figure 4.3 Cell viability assay of IONP-DTMs. Cells kept over 80% viability within the tested concentration range (0–625 μg mL^{-1}).

With the encouraging in vitro data, we moved to in vivo investigations to evaluate magnetic delivery with IONP-DTMs. To facilitate the particle tracking, we used ZW800, a near-infrared fluorescence dye, as a drug mimic. With near-infrared emission (ex/em: 780/800 nm), the migration and distribution of ZW800 can be traced in vivo. The “drug” loading is similar to that with rhodamine B. These IONP and ZW800 dually labeled diatoms were intravenously (i.v.) injected into 4T1 tumor xenograft models (1.65 mg/kg). A magnetic bar was attached to the skin of the tumors before the particle injection and was remained there for one hour. In the control group, no magnet was applied. No abnormalities of animals were observed through the diatom injection. After one hour, the magnet was removed and the animal was subjected to T2-weighted MR imaging. Compared to the pre-scan, no significant signal change was observed in the control group, indicating a minimal tumor accumulation. By contrast, a number of black areas appeared in tumors treated with a magnet (**Figure 4.4**). This signal drop in tumors was accredited to accumulation of IONPs that induce hypointensities. The MRI data correlates well with the in vivo fluorescence imaging results, finding dramatic difference in tumor uptake after 1 h (**Figure 4.4**). After the imaging, we sacrificed the animals and dissected tumors for ex vivo fluorescence imaging. With region-of-interest (ROI) analysis, it is revealed that more than 6.4 times more particles were accumulated in the tumors treated with a magnet, confirming the good efficacy of magnetic modulation.

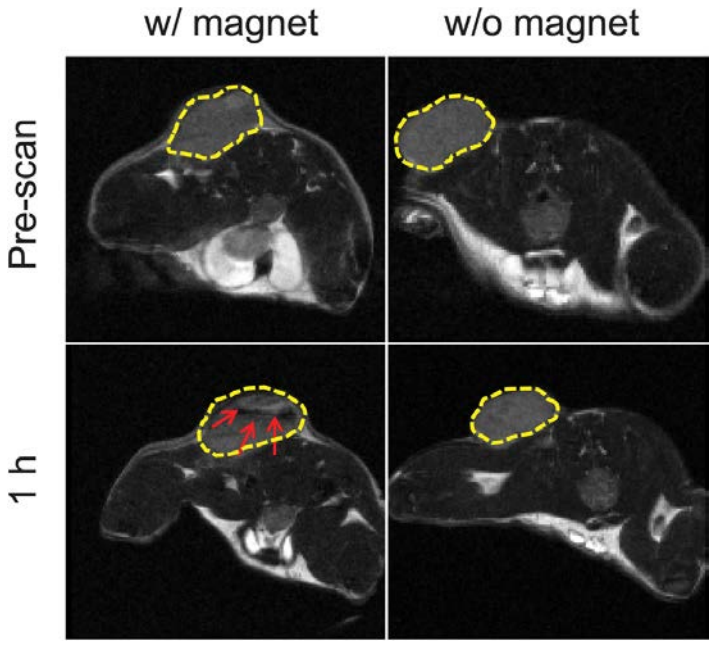

Figure 4.4 T2-weighted MR images taken prior to and 1 h after the injection of ZW800 loaded IONP-DTMs. Black areas (highlighted by red arrows) were observed in tumors where a magnet was attached to the tumor skin. By contrast, no signal change was observed if no magnet was applied.

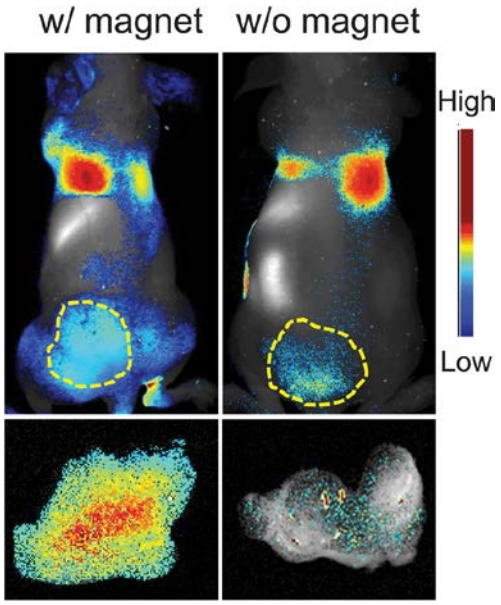

Figure 4.5 (Upper row) *in vivo* imaging results. Correlated to the MRI data, significantly more fluorescence signals were observed in tumors that were attached with a magnet. (Bottom row) *ex vivo* imaging with dissected tumors. Compared to the control, 6.4 times higher accumulation of diatoms was observed in the tumors that had been attached with a magnet during the process.

Conclusions

We demonstrated that IONP loaded diatoms could be used in vivo as magnetic delivery carriers. To our knowledge, this is the first example of the in vivo translation of diatoms. Significant improvement of tumor retention was observed when a magnetic field was applied to the tumor sites. This, together with the low toxicity and biodegradability of IONPs and diatoms, suggest the great potential of the technology. With their big size, diatoms are able to hold a broad range of functionalities. This includes loading multiple types of imaging functionalities for multimodality imaging. It is also possible to load a combination of therapeutics onto diatoms for cocktail cancer therapy. In the current investigation, small molecules were loaded onto diatoms through physical adsorption. Similar to common silica nanoparticles, the surface of diatoms can also be modified by organo-functional silanes to allow introduction of functionalities through covalent linkage. The related investigations are underway.[8]

In the present study, ~10 μm diatoms were used, which provided a good capacity for nanoparticle/molecule loading. This relatively large size, however, caused undesired particle accumulation in the lung, likely from trapped particles in the narrow capillaries (**Figure. 4.5**).[19–21] In future studies, it is important to develop size selection strategies to enrich small-sized diatoms, which may afford better pharmacokinetics. Also, the

relatively large pore size may cause a rapid release of drugs. This may be improved by introducing activatable stoppers that can block the pores and only be lifted in response to certain stimuli in tumors. Similar strategies have been applied to mesoporous silica nanoparticles with success.[22, 23] The related research is ongoing in our group.

Acknowledgements

This work is supported by the National Institutes of Health (5R00CA153772) and the National Science Foundation (CAREER DMR-0955908).

Supporting Information

Preparation of HSA-IONPs

5 mL of 15 nm IONPs at 1 mg/mL in chloroform were added to 20 mg of dopamine in 2 mL of DMSO. This mixture was mixed at 70°C for 1 hour. Hexane, as a poor solvent, was added and the particles were collected by centrifugation. The resulting particles were redispersed in 0.5 mL DMSO. 50 mg of HSA was dissolved in 1 mL of H_2O. The nanoparticle solution was added to the HSA solution dropwise while under sonication. The nanoparticles were purified by a NP-5 desalting column and redispersed in PBS.

Viability assay

Approximately 1×10^4 4T1 cells were seeded in each well of a 96-well plate. After 24 h incubation, IONP-DTMs at different concentrations (0, 37.5, 78, 156, 312, and 625 μg/mL) were added to the plate. After incubation for another 24 h, an MTT assay was performed to determine the cell viability.

Animal models

4T1 breast cancer model cells were cultured in MEM supplemented with 2 mmol/L L-glutamine, 1.5 g/L sodium bicarbonate, 0.1 mmol/L nonessential amino acids, 1.0 mmol/L sodium pyruvate, and 10% fetal bovine serum at 37 °C in a humidified atmosphere with 5% CO_2. Athymic nude mice were purchased from Harlan laboratories. The animal model was established by subcutaneously injecting approximately 1×10^6 4T1 cells into the right hind limb of each mouse. All the animal experimental procedures were conducted following a protocol approved by the University of Georgia Institutional Animal Care and Use Committee (IACUC).

In Vivo NIRF Imaging Studies

The imaging studies started when tumors reached a size between 200 and 500 mm^3. The 4T1 tumor bearing mice were anesthetized with isoflurane and intravenously injected with IONP-DTMs at a dose of 1.65 mg/kg. Before injection, a magnet bar was attached to the skin of the tumors, and remained there for 1 h. For control animals, no magnetic bar was applied. T_2-weighted fast spin echo images were acquired on a 7 T Varian small animal MRI system before and 1 h post the particle injection, with the following scan parameters: TR = 2.5 s; TE = 48 ms; ETL = 8; FOV 40 2 mm^2; matrix size = 2562 ; 15 axial slices with 1 mm slice thickness. Fluorescence studies were performed on a Maestro II imaging system (PerkinElmer). After the imaging, the animals were sacrificed. Tumors were harvested and subjected for ex vivo imaging. The images were unmixed by the vendor provided software. ROIs were circled around the tumors, and the optical intensities (in total scaled counts/s) were read by the Maestro software.

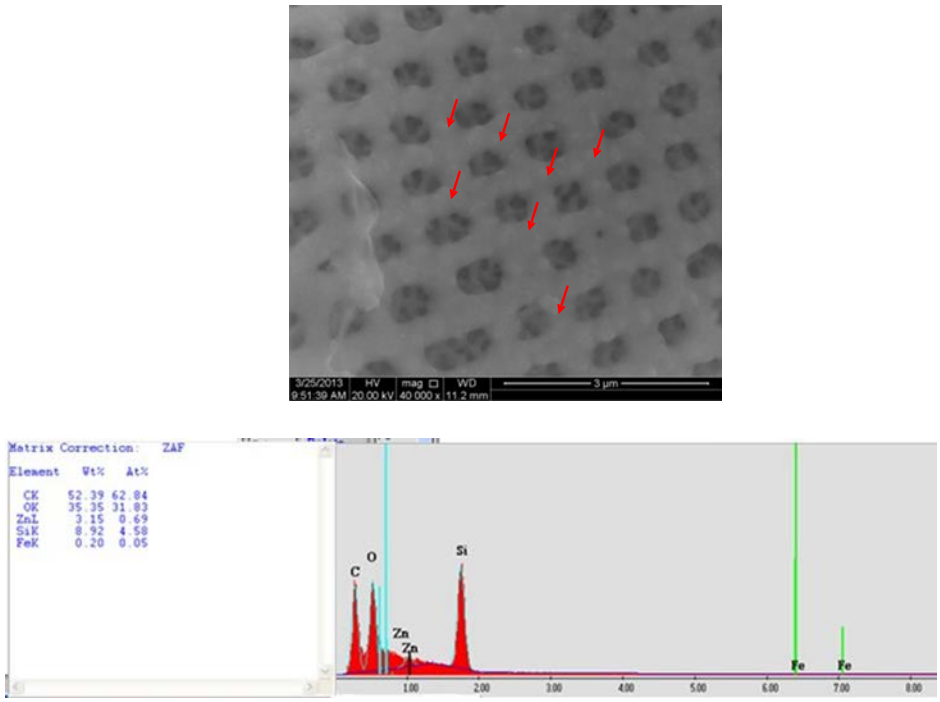

Figure 4.6. a) SEM image of IONP-DTM. b) EDX analysis of IONP-DTMs.

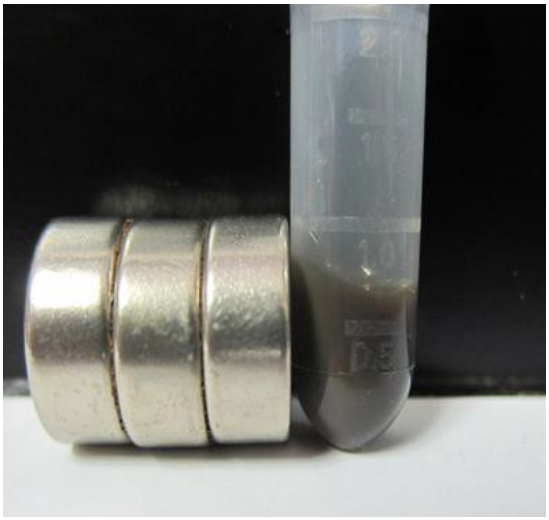

Figure 4.7. Applying a magnetic bar to a HSA-IONP solution. Due to weak magnetic response, most of the particles were not attracted to the wall.

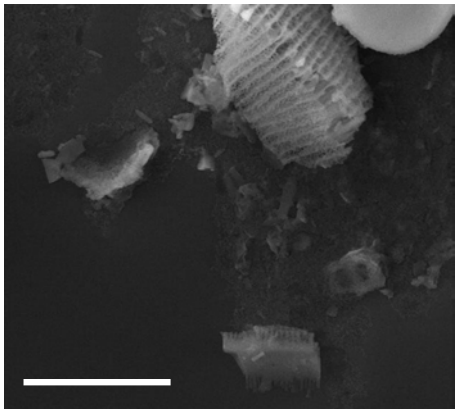

Figure 4.8. IONP-DTMs after one week incubation in a body fluid mimic. Many particles were found partially degraded after the incubation.

Notes and References

(1) R. Siegel, D. Naishadham and A. Jemal, *Ca-Cancer J. Clin.*, 2012, **62**, 10–29

(2) L. Brannon-Peppas and J. O. Blanchette, *Adv. Drug Delivery Rev.*, 2012, **64**, 206–212

(3) H. Maeda, G. Y. Bharate and J. Daruwalla, *Eur. J. Pharm. Biopharm.*, 2009, **71**, 409–419J.

(4) Fang, H. Nakamura and H. Maeda, *Adv. Drug Delivery Rev.*, 2011, **63**, 136–151

(5) C. Barbe, J. Bartlett, L. G. Kong, K. Finnie, H. Q. Lin, M. Larkin, S. Calleja, A. Bush and G. Calleja, *Adv. Mater.*, 2004, **16**, 1959–1966

(6) Q. J. He and J. L. Shi, *J. Mater. Chem.*, 2011, **21**, 5845–5855.

(7) J. Lu, M. Liong, Z. X. Li, J. I. Zink and F. Tamanoi, *Small*, 2010, **6**, 1794–1805 .

(8) I. I. Slowing, J. L. Vivero-Escoto, C. W. Wu and V. S. Y. Lin, *Adv. Drug Delivery Rev.*, 2008, **60**, 1278–1288.

(9) U. Prabhakar, H. Maeda, R. K. Jain, E. M. Sevick-Muraca, W. Zamboni, O. C. Farokhzad, S. T. Barry, A. Gabizon, P. Grodzinski and D. C. Blakey, *Cancer Res.*, 2013, **73**, 2412–2417.

(10) H. Maeda, *Proc. Jpn. Acad., Ser. B*, 2012, **88**, 53–71.

(11) X. Huang, X. Peng, Y. Wang, Y. Wang, D. M. Shin, M. A. El-Sayed and S. Nie, *ACS Nano*, 2010, **4**, 5887–5896.

(12) C. W. Lu, Y. Hung, J. K. Hsiao, M. Yao, T. H. Chung, Y. S. Lin, S. H. Wu, S. C. Hsu, H. M. Liu, C. Y. Mou, C. S. Yang, D. M. Huang and Y. C. Chen, *Nano Lett.*, 2007, **7**, 149–154.

(13) D. K. Yi, S. T. Selvan, S. S. Lee, G. C. Papaefthymiou, D. Kundaliya and J. Y. Ying, *J. Am. Chem. Soc.*, 2005, **127**, 4990–4991.

(14) D. Losic, Y. Yu, M. S. Aw, S. Simovic, B. Thierry and J. Addai-Mensah, *Chem. Commun.*, 2010, **46**, 6323–6325.

(15) J. Xie, J. Wang, G. Niu, J. Huang, K. Chen, X. Li and X. Chen, *Chem. Commun.*, 2010, **46**, 433–435.

(16) T. L. Liu, L. L. Li, X. Teng, X. L. Huang, H. Y. Liu, D. Chen, J. Ren, J. Q. He and F. Q. Tang, *Biomaterials*, 2011, **32**, 1657–1668.

(17) Q. M. Quan, J. Xie, H. K. Gao, M. Yang, F. Zhang, G. Liu, X. Lin, A. Wang, H. S. Eden, S. Lee, G. X. Zhang and X. Y. Chen, *Mol. Pharm.*, 2011, **8**, 1669–1676.

(18) Q. J. He, J. L. Shi, M. Zhu, Y. Chen and F. Chen, *Microporous Mesoporous Mater.*, 2010, **131**, 314–320.

(19) L. Illum, S. S. Davis, C. G. Wilson, N. W. Thomas, M. Frier and J. G. Hardy, *Int. J. Pharm.*, 1982, **12**, 135–146.

(20) A. Delgado, I. Soriano, E. Sanchez, M. Oliva and C. Evora, *Eur. J. Pharm. Biopharm.*, 2000, **50**, 227–236.

(21) N. Willmott, Y. Chen, J. Goldberg, C. Mcardle and A. T. Florence, *J. Pharm. Pharmacol.*, 1989, **41**, 433–438.

(22) C. L. Zhu, C. H. Lu, X. Y. Song, H. H. Yang and X. R. Wang, *J. Am. Chem. Soc.*, 2011, **133**, 1278–1281.

(23) S. Bhattacharyya, H. Wang and P. Ducheyne, *Acta Biomater.*, 2012, **8**, 3429–3435.

Chapter 5

CONCLUSIONS AND FUTURE WORK

Summary

The focal purpose of the research presented in this dissertation is reporting the development of alkali halide nanoparticle mediated ion delivery. This class of nanoparticles has never been reported in the literature for biomedical applications. Nor have nanoparticles been used as a means of alkali ion delivery. The asymmetric ion gradients that exist across cell membranes are among the most carefully maintained functions in biology. Disruption of these gradients is associated with compromised cellular function and death. While there are molecules that can induce altered ion balance, they suffer from poor bioavailability and display off-target toxicity.

We developed sodium chloride nanoparticles to ameliorate the issues with ion delivery. By using a novel synthesis in non-polar organic solvents we were able to produce NaCl cubes with an edge length of 50-100 nm. The particles are coated with phospholipids imbuing them with temporary aqueous stability. The particles display a concentration dependent toxicity to cells that appears to be most closely associated with classical necrosis pathways. Increase of both intracellular sodium and potassium suggests uptake of the nanoparticles. Coincident with ion uptake, we see labeled nanoparticles enter the cells. Further proof that it is the nanoparticle state of NaCl that induces damage is seen by delayed addition of NaCl NPs suspended in aqueous solutions. NaCl toxicity is greatest when immediately administered to cells. If the

particles are allowed to rest in PBS their toxicity progressively decreases. Though coated with a phospholipid layer, nanoparticles quickly dissolve when suspended in water as seen by TEM. ATP depletion, loss of mitochondrial membrane potential, and aggregation of mitochondria are all indicative of severe damage to the mitochondria. Given these attributes, we chose to proceed with a proof-of-concept study in a breast cancer model. It was found that the nanoparticles could slow the growth of tumors and reduce the size by nearly three-fold over two weeks.

The other main project detailed in this dissertation is ion delivery using lithium fluoride nanoparticles. Rather than killing cells, in this project we aim to protect the integrity of the chondrocytes in the joint space. Recent reports have demonstrated that lithium could provide protection from osteoarthritis. However, OA is a local disease and systematic administration of lithium yields concentrations that are very close to toxic levels. While direct injection of lithium to the joint has been shown to increase therapeutic efficacy, the very small size of the drug suggests rapid dispersion from the disease site.

We hypothesized and found that silica-coated lithium fluoride nanoparticles could slowly release lithium from the joint space. Lithium fluoride particles were synthesized by a simple precipitation reaction and were subsequently coated with silica. These particles release Li^+ over two days compared to 1 hour with uncoated particles. Concerns with release of fluoride in the joint space were assuaged by the rapid sequestration of fluoride by extracellular calcium. The particles were found to be minimally toxic over the used concentration range. They were also able to match or exceed the therapeutic effect of LiCl in down-regulating catabolic markers when cells

were exposed to inflammatory cytokines. Coated particles were injected into OA animal joint models with the FDA approved pain drug hyaluronic acid. It was found that this joint therapy was better than HA injections alone and was 10x more effective than LiCl and HA injections.

Future Work

These particles should be viewed as only the baseline of what nanoparticle-mediated ion delivery can accomplish. Perhaps the greatest challenge to obtaining regulatory approval for new drugs and imaging agents is concerns over toxicity[1]. This is especially true for inorganic nanomaterials because of their long lifetimes in the body. Alkali halide nanostructures inherently completely and rapidly dissolve into constituent ions. By judicious choice of non-toxic component ions, this can effectively negate concerns over long term toxicity. These criteria alone suggests six possible formulations that should display minimal toxicity: LiCl, LiI, NaCl, NaI, KCl, and KI. Also, depending on the purpose, fluoride may be viewed to display an acceptable level of risk.

When only considering NaCl nanoparticles the possibilities are extensive. We described two processes for synthesis of these particles and a single coating technique. Introduction of a more solid coating to slowly release ions could abolish the toxicity of these particles. It is also possible that an activatable coating could allow high uptake into tumors using i.v. injection. Subsequent burst release, inducing cell death in a temporal and spatially specific manner could be achieved. We demonstrated that loading a dye into the coating allows tracking of these particles. Numerous other dyes or imaging modalities could be introduced onto the surface of the particles and used for

in vivo imaging. Given the potential, the immediate goal of research into NaCl particles is controlling particle stability. Oleylamine is assumed coat the particles by electrostatic attraction to surface chlorides on the nanoparticle. Development of a stronger and more effective bond to the particle surface will allow for significant increase in the stability of the particles.

When considering future work for LiF the options appear to be more localized. Facile altering of silica coating thickness would change the rate of dissolution allowing for slow or burst release behavior. As mentioned in Chapter 1, Lithium has many effects in vivo through its inhibition of GSK-3 and other enzymes. It has been suggested that lithium sensitizes radiotherapy resistant cells to new therapy[2]. Introduction of rapidly degrading LiF to a tumor may combine the effects of NaCl particle therapy with the effects of lithium. Despite demonstrating the ability of extracellular calcium to sequester fluoride, concerns remain over its ultimate safety. Using chloride as the counter anion is one possibility, but LiCl exhibits a solubility that is significantly higher than LiF's[3].

Of the other potential formulations for alkali halide nanoparticles the ones composed of iodide are the most immediately interesting. Iodide has been suggested as an imaging modality for years. In fact the first CT contrast agent was sodium iodide[4]. Yet, the high number of side effects prevented the further use of alkali halide salts for imagine. Instead, research focused on benzene based iodide derivatives[5]. However, it is difficult to introduce significant amounts of iodide into a small molecule and maintain favorable pharmacokinetic attributes. Several nanoformulations containing iodide have been suggested[6]. These particles could relieve some of the issues with small molecule

imaging, but still have relatively low loading rates or poor solubility. An alkali iodide nanoparticle, as a carrier of iodide, could potentially be a highly effect CT contrast agent by combining the benefits of both small molecules and nanoparticles. As with LiCl, though, the high solubility of such a formulation is problematic.

Though a new field, ion delivery mediated by alkali halide nanoparticles has the potential to provide a significant positive impact to both the research carried out in the biomedical field and to patients who are seeking therapy for their afflictions. It is with this hope that the contents of the proceeding manuscript have been written.

References

(1) Johnson, J. R.; Williams, G.; Pazdur, R. *J Clin Oncol* **2003**, *21*, 1404-1411.

(2) Rouhani, M.; Goliaei, B.; Khodagholi, F.; Nikoofar, A. *Arch Iran Med* **2014**, *17*, 352-360.

(3) Friend, J. N.; Hale, R. W.; Ryder, S. E. A. *J Chem Soc* **1937**, 970-970.

(4) Osborne, E. D.; Sutherland, C. G.; Scholl, A. J.; Rowntree, L. G. *Jama-J Am Med Assoc* **1983**, *250*, 2848-2853.

(5) Lusic, H.; Grinstaff, M. W. *Chem Rev* **2013**, *113*, 1641-1666.

(6) Lee, N.; Choi, S. H.; Hyeon, T. *Adv Mater* **2013**, *25*, 2641-2660.